Fatigue Testing and Analysis of Aluminum and Steel Partial Joint Penetration (PJP) Welds for Bridge Applications

by

Abdullah Abdelbadie

A thesis
presented to the University of Waterloo
in fulfillment of the
thesis requirement for the degree of
Master of Applied Science
in
Civil Engineering

Waterloo, Ontario, Canada, 2023

Author's Declaration

I hereby declare that I am the sole author of this thesis. This is a true copy of the thesis, including any required final revisions, as accepted by my examiners. I understand that my thesis may be made electronically available to the public.

Abstract

Partial joint penetration (PJP) welds are a cost-effective alternative to full penetration welds and have certain advantages, especially in situations where a full penetration weld is unnecessary and the stress on the weld is low. Unfortunately, these welds are typically fatigue prone, and determining the fatigue stress limit for PJP welds, and similarly for aluminum partial penetration flare bevel groove (FBG) welds, is challenging because the available methods are either untested in these applications or overly complex. PJP welds are also useful in situations where full penetration welds are impractical, such as in thin components like rib-deck welds of orthotropic steel decks (OSDs) where weld defects can result if a full penetration weld is attempted. Current provisions in CSA S6-19 Clause 10.16 require the design of OSDs to satisfy the requirements of Clause 9.8.3 of AASHTO LRFD Bridge Design Specifications while still using loads and factors from CSA S6-19 for the fatigue limit state (FLS). Due to the difference in applied factors and loads, there are instances when attempting to use this approach incorrectly can lead to possible negative outcomes from the point of view of structural safety or economy. For example, in the fatigue design, it is not clear when to switch from the AASHTO provisions (for analysis) to the CSA provisions (to account for the Canadian truck traffic). This issue raises serious concerns, which may discourage designers in Canada from employing OSD solutions and thus harnessing their benefits in new bridge projects and applications involving service life extension of existing bridges.

Against this background, a study was conducted to address current gaps in the literature concerning the fatigue performance of PJP and partial penetration FBG welds in bridge applications.

The experimental fatigue testing of 19 T-joint aluminum FBG welded specimens, conducted within the scope of this study, yielded valuable insights into the fatigue behavior of these components. Notably, the effective throat was found to be the most important factor influencing the performance of FBG welds, and it was found that precision in the welding execution is crucial. An SN curve was established based on the experimental results for a 95% survival probability. The weld performance based on the design curve was found to be similar to Detail Category E in CSA S6-19. Linear elastic fracture mechanics (LEFM) methods were then used, along with a 3D finite element (FE) model, to supplement the experimental study and predict the fatigue performance of the tested aluminum FBG welds.

Lastly, an investigation was conducted on OSD rib-deck welds to determine how the transverse wheel location affects the stress at the root and toe. In order to address the ambiguity issues identified in CSA S6-19, the local stresses resulting from Canadian and American trucks were computed and compared to demonstrate the correct use of the appropriate factors required for fatigue design.

Acknowledgements

I would like to express my sincere gratitude to my supervisor, Scott Walbridge, for his invaluable guidance and support throughout my thesis project. Scott has been an incredible mentor and teacher, sharing his wealth of knowledge and experience in civil engineering and professional development. His patience and kindness have made a tremendous difference in my academic experience, and I am thankful to have had the privilege to work with such an exceptional supervisor.

I would like to take this opportunity to express my upmost appreciation to my father Gamal Nazmi Abdelbadie for his unwavering support and guidance throughout my life. From an early age, my father instilled in me a passion for engineering and encouraged me to pursue my dreams. He has always been there for me, providing me with wise advice and guidance throughout every step of my academic and professional journey.

The assistance of the skilled technicians from the structure laboratory - namely, Richard Morrison, Robert Kaptein, Victor Lewis, and Peter Volcic - was crucial in making this undertaking possible.

I am thankful for having a friendly and motivating research group: Dr. Ali Chehrazi, Mohammad Barkhori Mehni, Michelle Chien, and Dr. Mohamed Tolou. The intellectual and personal discussions they shared with me have made my experience at UW delightful.

I would like to express my appreciation to the Canadian Standards Association (CSA) and the MITACS Fellowship Program for their financial backing in this research. I also extend my gratitude to the CSA Project Advisory Panel, as well as other members of the CSA S6 technical committees who provided their invaluable advice and input in this undertaking.

Table of Contents

List of Figures

List of Tables

1 Introduction

1.1 Background

Partial joint penetration welds (PJP) are welds that do not extend fully through the thickness of the material being joined. Instead, the weld only penetrates part of the way through the material. PJP welds are often used in situations where a full penetration weld is not required, such as in joints where the stress on the weld is not significant, or where significant cyclic loading is not anticipated.

PJP welds can also be used in situations where a full penetration weld is difficult or impractical to achieve, such as when welding very thin components with no backing, where using a full penetration weld can result in defects such as weld blow-through. PJP welds require less material and less surface preparation and are typically more economical than full penetration welds. In general, however, full penetration welds have much better fatigue performance than PJP welds. This is because full penetration welds result in a more uniform and continuous connection, with a lower stress concentration at the end of the weld. However, it is important to note that the actual fatigue performance of both full penetration and partial penetration welds will differ greatly depending on various factors such as the welding parameters, loading conditions, and failure location (toe or root). Consequently, depending on these factors, prediction of fatigue performance may require different fatigue analysis techniques.

PJP welds can be used in the construction of steel bridges, particularly for non-critical areas of the bridge where the loads and stresses are relatively low. Partial penetration flare bevel groove (FBG) welds in pedestrian bridges made out of hollow structural sections (see Figure 1.1a) are an example where the use of one type of PJP weld is common. The use of PJP welds in bridge construction can offer some benefits, such as reduced fabrication costs and faster construction times. Some examples of areas where PJP welds may be used in bridge construction currently include the fabrication of non-critical connections such as diagonal bracing, secondary framing, and cross frames. PJP welds can also be used in the splicing of steel plates or sections. If fatigue performance is a critical consideration for a particular application, it is generally recommended to use full penetration welds. However, if a PJP weld is required, it is important to carefully design the joint and control the welding parameters to minimize the risk of fatigue cracking. Unfortunately, the literature does not provide much guidance for the fatigue analysis of PJP welds, particularly for the analysis of aluminum PJP flare bevel groove (FBG) welds.

Orthotropic Steel Decks (OSDs – see Figure 1.1b) consist of a thin plate supported by floor beams typically oriented perpendicular to the traffic direction, with longitudinal ribs stiffening the plate. The

resulting structural system has different properties in the directions parallel and perpendicular to the flow of traffic.

OSDs represent an efficient, relatively lightweight deck system that lends itself to applications where minimization of the dead load is of great importance. Furthermore, they require very little maintenance throughout their service life and therefore are therefore appropriate for structural applications where access to the deck would be difficult. The typical deck configurations have minimal joints that decrease the risk of leaking due to de-icing salts and can be standardized for modular applications, promoting rapid constructability compared to other conventional construction types [1].

Figure 1.1: a) Aluminum pedestrian bridge in Brossard, QC, b) Murray Street Bridge OSD, ON.

The ribs in OSDs are typically thin-walled U-sections and are connected to the deck plate through a PJP fillet weld instead of a full penetration weld to avoid "blow through" – a serious type of weld defect. A common challenge when analyzing OSDs is representing the stresses in the critical regions surrounding the welds, which is essential for the fatigue analysis of the connection. Furthermore, case studies [1-22] have shown that fatigue in the welds is often a critical failure mode for OSDs.

Current provisions in CSA S6-19 Clause 10.16 [23] require the design of OSDs to satisfy the requirements of Clause 9.8.3 of AASHTO LRFD Bridge Design Specifications [24], while still using loads and factors from CSA S6-19 for the fatigue limit state (FLS). Due to differences in the applied factors and loads, there are instances where attempting to use this approach incorrectly (which can happen, due to lack of clarity in several places in the CSA provisions) can lead to possible negative outcomes from the point of view of structural safety or economy. For example, in fatigue design, it is not clear when to switch from the AASHTO provisions (for analysis) to the CSA provisions (to account for differences in Canadian truck traffic). This issue raises serious concerns, which may discourage designers

in Canada from employing orthotropic deck solutions and thus harnessing their benefits in new bridge construction projects and applications involving service life extension of existing bridges.

1.2 Objectives

Against this background, the objectives of the project presented in this thesis are as follows:

1) to perform fatigue tests on aluminum hollow structural section (HSS) T-joints with partial penetration FBG welds, to collect experimental fatigue data for this connection type,
2) to use various existing methods to predict the fatigue performance of the tested joints and assess the suitability of each method as a practical design tool, and
3) to use similar prediction methods to perform fatigue design of an OSD system with PJP joints, so the suitability and limitations of each method can be assessed for this application.

1.3 Scope

The scope of this research is limited to aluminum and steel welds intended for bridge elements and applications including pedestrian bridges made with welded aluminum hollow structural section (HSS) T-joints and orthotropic steel bridge deck (OSD) for vehicular bridge applications.

2 Literature Review

A literature review has been conducted on the performance and evaluation of aluminum partial penetration FBG welds, and steel PJP welds in orthotropic bridge decks. The key findings are summarized in the following sections of this chapter.

2.1 Aluminum Partial Penetration Flare Bevel Groove (FBG) Welds

2.1.1 Aluminum Applications in Structures

In construction, aluminum presents itself as a viable material option where reduction of self weight is paramount such as curtain walls, aluminum's density is roughly a third of that of steel, or in environments that are corrosive due to aluminum's corrosion resistant properties. However, its initial cost is roughly three times that of steel. Recent advancements in research and technology have shown through life cycle analysis that aluminum requires considerably less maintenance than its steel alternatives throughout the service life of the structures. Pedestrian bridge applications are another setting that exemplifies the advantages of aluminum that reduce the maintenance cost and weight of the structure, allowing this material choice to increasingly become the more viable material choice. A study has shown that over a lifespan of 50 years, aluminum is more economical material choice than steel for the construction of pedestrian bridges due to the consideration of the running costs throughout the structure's service life [25]

2.1.2 Aluminum Performance in Welding

Aluminum structural members are typically constructed of 6061 alloys which are weldable with similar techniques to welding of steel. A major difference in the response of aluminum to welded compared to steel is the localized material properties change due to the heat. The welding process typically requires exposure of the metal in the region of the weld to extremely high temperature which is also referred to as the Heat Affected Zone (HAZ). The severe temperature rises results in the HAZ to experience large compromise in their strength capacity that can go up to 50% [26].

FBG welds occur when a straight surface is welded to a curved one as shown in the following image. The connection of interest in this study is a FBG weld between the straight face of a hollow square structural member and its beveled corner in a T-joint configuration.

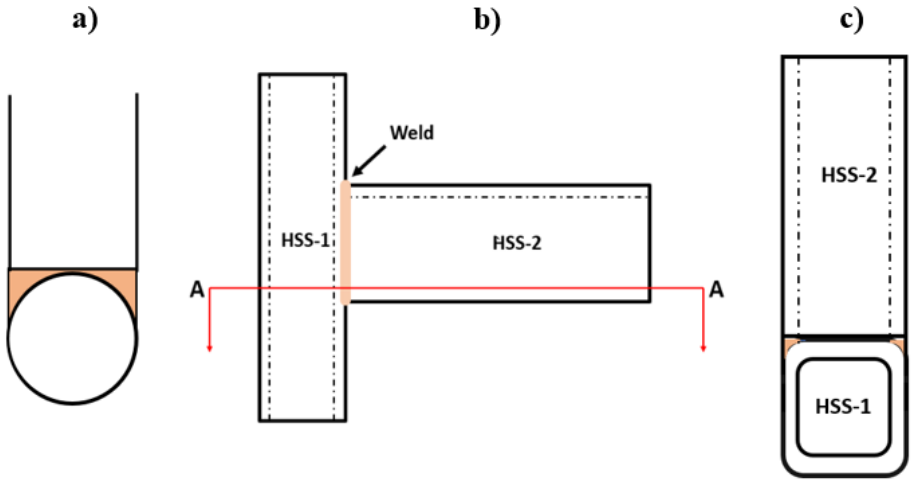

Figure 2.1: a) Typical FBG Weld. b) FBG weld for two HSS members, c) Cross section view of welded HSS.

FBG welds are a type of connection that can be used in truss bridges consisting of hollow structural sections (HSS). The cost of these connections can be reduced by welding the joints without beveling them first, which negatively impacts the fatigue performance of the connection. This is a popular solution in steel and aluminum pedestrian bridge applications, where the severity of the cyclic loading from a fatigue perspective is currently not well understood. To further investigate this issue, a study was conducted on the fatigue behavior of FBG welds in T-joints made of aluminum square HSS members. The typical weld is a penetration weld which has a higher cost but a better fatigue performance, this study is primarily concerned with investing the fatigue performance of PJP FBG welds.

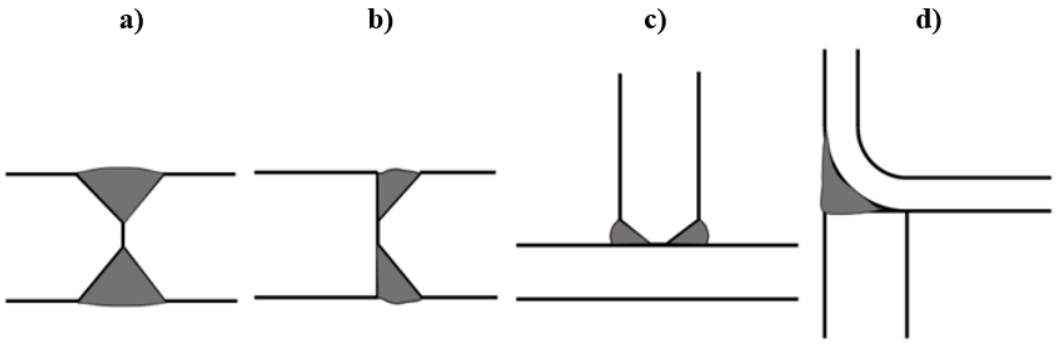

Figure 2.2: a) Double-bevel PJP Butt Weld, b) Single-Bevel Groove Weld, c) T-Type PJP Weld, d) FBG Weld [27].

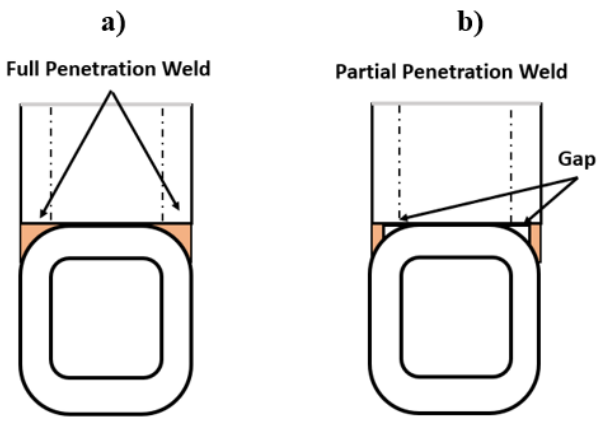

Figure 2.3: a) Complete joint penetration FBG weld b) PJP FBG weld.

2.1.3 Fatigue in Metallic Structures

Fatigue failure occurs when a member failure due to its exposure to a repeated loading that is much less than its static capacity. In the context of metals, fatigue typically occurs in regions where there are stress concentrations that can result from a variety of reasons including residual stresses or geometric irregularities which are both characteristics of welds. A small microcrack(s) grows in the region of the stress concentration and grows into a macroscopic crack in a transition that is referred to as the crack initiation phase. The macroscopic crack continues to propagate at an increasing growth rate under the repeated loading in the crack propagation phase until the remaining material can no longer resist the applied load which is the point at which fatigue failure is said to have occurred. The increasing crack growth rate can often result brittle failure modes without warning which limits the end user's ability evacuate the structure or reactive maintenance in the event of severe damage.

2.1.4 Fatigue in Bridges

When it comes to bridges, literature commonly refers to fatigue as the primary cause of failure in structures or at least on of the major causes of failure in bridges. A study by ECCS [28] shows fatigue as the most common cause of structural damage resulting in 38% of failure in metallic. Another study shows

fatigue and fracture comprising of 80-90% of failure in steel bridges [29]. Therefore, fatigue assessment is paramount to ensure safe bridge design of structures.

2.1.5 Fatigue Assessment in Structures

Fatigue in structures can either be high cycle fatigue which occurs around 500,000 cycles or more and low cycle fatigue which occurs around 10,000 cycles. Low cycle fatigue is commonly used in seismic assessment of structures, these applications typically require non-linear material properties and deal with large deformations. High cycle fatigue often deals with low deformations occurring at loads much less than the static strength of the member (about 50% if the static capacity or less). Fatigue induced in bridges which is the focus of this study, is induced by trucks passing at average annual daily traffics ranging from 100s to 1000s of trucks a day making high cycle fatigue the appropriate case for fatigue analysis. Consequently, linear elastic material properties can be used in the analysis of these applications.

The realistic representation of fatigue loading applied on a bridge requires accounting for the different weights of trucks, and cars that may be passing by, which requires the use of variable amplitude loading (VA). Fatigue analysis using VA is afterwards, requires equating the varying loads to a single amplitude through different techniques exemplified by Miner's sum. In experimental practice, using VA loading can be quite rigorous in defining a reasonable case that is a realistic representation of a single bridge while misrepresenting others. Therefore, in experimental applications, its more convenient to implement constant amplitude fatigue (CA) as it is easier to implement in a test setup and is more general for multiple bridge applications.

A representation of CA loading throughout the testing of a component can be shown by the following component where the maximum and minimum stresses are σ_{max} and σ_{min}, the alternating stress σ_a, and mean stress σ_m can be defined as

$$\sigma_a = \frac{\sigma_{max} - \sigma_{min}}{2} \tag{2.1}$$

$$\sigma_m = \frac{\sigma_{max} + \sigma_{min}}{2} \tag{2.2}$$

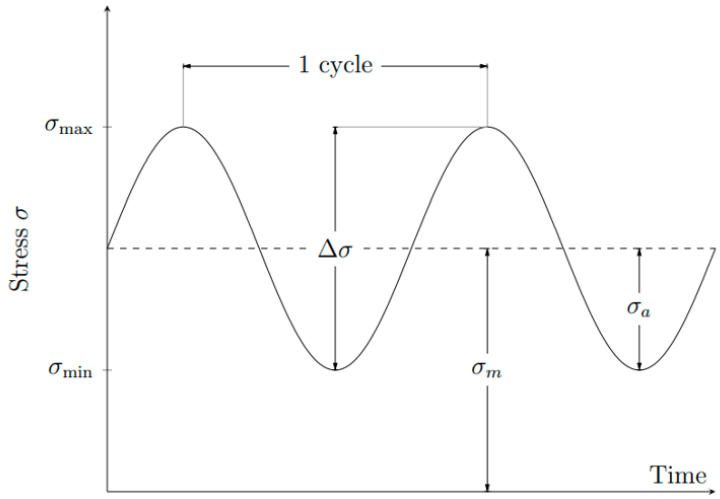

Figure 2.4: Typical stress versus time curve for constant amplitude loading [26].

Assuming the connection is under tension during the entire loading process, as tension-only loading is more severe than cycling from tension to compression or compression-only loading, both σ_{max} and σ_{min} will be positive. The ratio of σ_{min} over σ_{max} is referred to as the stress ratio and is kept constant throughout the entire testing procedure for different load ranges.

2.1.6 Methods of Structural Analysis of Fatigue

The two most common approaches for high cycle fatigue assessment of metals are the use of empirical charts referred to as SN curves (also referred to as stress-life approach) or carrying out an analytical assessment which commonly employs finite element analysis FEA.

2.1.7 SN Curves

SN-curves are generated from large scale tests caried out in laboratories to provide curves that specify the performance of a certain geometric configuration under CA loading. The data obtained from the tests is plotted on a log -log chart and a line of best fit is generated through the data. A design curve is afterwards obtained by shifting the line of best fit downwards to obtain a survival probability of 95%. These curves can be used to evaluate a connection of a similar geometric configuration by simply identifying the stress range that will be applied and locating the corresponding fatigue life or vice versa. A typical design curve takes the following exponential form.

$$\Delta\sigma = \left(\frac{C}{N_f}\right)^{\frac{1}{m}} \tag{2.3}$$

where $\Delta\sigma$ is the difference between σ_{max} and σ_{min}, N_f is the number of load cycles until failure, m is the slope if the data on the log-log plot and C is a constant that is specific to the S-N curve. In the case of the CSA S-157, the SN curves are compiled in the 5 different Categories A through E and lists of connections and configurations are related to the category of the closest performance.

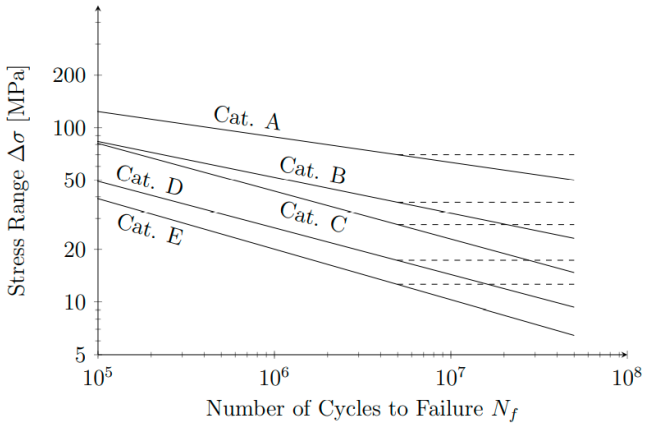

Figure 2.5: SN-curve with detail categories shown obtained from CSA S-157 [29].

2.1.8 Finite Element Analysis

Analytical techniques for analysing the fatigue performance of welded connection often leverage FEA and include the use of linear elastic fracture mechanics, hotspot stress method, and stress notch approach. These approaches will each be further elaborated on in Section 2.2.3.

2.1.9 PJP in International Design Codes

A comparison was made between the design considerations for PJP groove welds in load bearing applications for aluminum outlined by international design codes from Canada, United states and Europe. The Canadian design codes of interest were the CSA standard S157 - Strength Design in Aluminum Structures [29], CSA standard S6 - Canadian Highway Bridge Design Code [23]. The American standard of most relevance was The Aluminum Design Manual (ADM) [28] while the relevant European standard was Eurocode 9: Design of aluminium structures [30].

CSA S157 [29]: If the welds were made using GMAW or GTAW and the groove opening angle is higher than 60^{o} then the effective throat can be equated to the groove preparation depth.

- CSA S157 Advises against the use of PJP groove welds for load bearing connections as per CL 15.2.1.
- Minimum groove angle for their applications is $60^{o.}$

CSA S6 [23]: Partial penetration welds are strictly prohibited for load carrying connections.

ADM [30]: The strength of the weld is reduced by 40% to consider the effects of notching due to the incomplete penetration.

Eurocode 9 [31]: PJP welds are limited to applications in secondary and non load bearing members and requires their effective throat to be found.

2.1.10 Design Fatigue SN Curves for PJP Aluminum Welds

No design curves are recommended explicitly for PJP applications however, Eurocode 9 [31] and International Institute of Welding [39] provide design S-N curves for their applications. Comparison between the proposed S-N curves and those of the CSA S157 [29] has shown the closest comparable performance is that of a Category E.

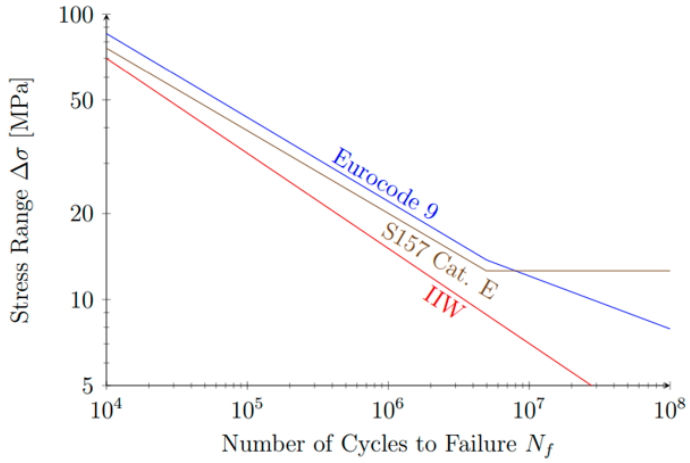

Figure 2.6: Comparative S-N curve between IIW recommendations, CSA S-157, and Eurocode performance on the predicted performance of PJP welds [27].

2.1.11 Fatigue Analysis of PJP Welds in Steel

Studies concerned with PJP welds mostly look in applications for steel in butt joint applications such as [32-34] which look into the effect of lack of penetration of the weld on the fatigue performance of the specimen. A typical study consists of a experimental program and a supplementary FEM analysis through linear elastic fracture mechanics or the stress notch approach. [32] is a study that looks into the effect of the seam size for partial penetration a single- and double-sided weld which are not permissible for fatigue prone applications and investigates their fatigue performance and evaluability. The study concluded that the fatigue performance of the PJP is evaluable through the stress notch approach with reasonable accuracy, and depending on the seam size, practical applications exist where the cost-saving advantage of these welds can be leveraged while maintaining safe design. [33-35] conducted an experimental study on PJP steel butt welds and concluded that as the lack of penetration increases, the fatigue performance drops severely however results form a LEFM analysis in study [35] show that the fatigue life of the connection can be evaluated successfully for different levels of penetration through LEFM.

2.1.12 PJP Weld in Aluminum

[27] is a master's thesis that thoroughly investigates the fatigue performance of 6061 (commonly used in civil engineering applications) Aluminum PJP butt welds through experimental testing and FEM. The

experimental program consisted of 56 fatigue life tests at varying degrees of penetration and developing a LEFM model to represent the crack behavior of the specimen. The study looked into the effect of the heat affected zone, weld roughness and lack of penetration.

[36] is an experimental study of 100 butt welded aluminum specimen with 5083 base alloy with varying degrees of penetration and varying thicknesses. [36-37] were studies with interest directed towards vehicle aluminum components that looked into PJP weld through testing welded specimens at varying degrees of penetration.

The conclusions drawn from the studies can be summarised as follows:

- Degree of penetration is not influential on the fatigue performance if the stress definition considers the net weld cross section and is measured accurately suggesting that S-N curves are appropriate for assessment. [26]
- However, the study also showed that certain unintended weld defects such as accidental eccentricity from warping can detrimentally reduce the fatigue performance of the connection [26].
- The base metal thickness has little influence over the fatigue performance of the specimen [35-38].
- The performance of the welded specimens is governed by the degree of penetration [35-38].

2.2 Fatigue in Orthotropic Steel Decks

In the following subsections of this chapter, literature is reviewed on the challenges surrounding fatigue design and performance assessment for PJP welds in orthotropic steel deck (OSD).

2.2.1 Commonly Reported OSD Fatigue Crack Types

The welded rib-to-deck joints in OSDs are susceptible to fatigue cracking. Four fatigue crack types can occur in the rib-to-deck joints. These crack types include: a) a weld root crack that propagates through the deck plate (root-deck crack), b) a weld root crack that propagates through the weld throat (root-weld crack), c) a crack that propagates from the weld toe on the rib through the rib wall thickness (toe-rib crack), and d) a crack that propagates from the weld toe on the deck underside through the deck plate (toe-deck crack). All four of these typical crack types are shown in Figure 2.7 [2-5].

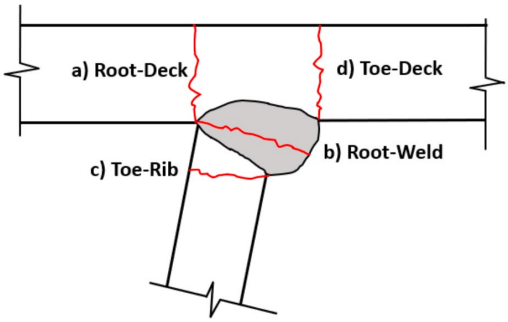

Figure 2.7: Types of potential fatigue cracks in rib-deck welds of OSDs.

Fatigue testing of OSDs is generally done in one of three types of experiments the single weld test specimen, the single U-rib test specimen, and the large-scale test specimen with several U-ribs. The choice of the experiment type influences the fatigue mode of failure observed, as different modes of failure can dominate different experiment types. The prominent failure mode for single weld-tested specimens is cracking in the root-deck crack [3-5], while fatigue tests on single U-ribs have been reported to experience weld toe cracking that propagates to the deck plate [2,9-10]. Large-scale testing of OSDs yielded both types of fatigue cracking depending on the loading method [11-13]. Single weld tests are suitable for assessing the impact of the welding process on fatigue behaviour while lacking the collective representation of OSDs as a structural system. Single U-rib experiments capture the integral behaviour of OSDs however, the prominently reported mode of failure of toe cracking deviates from more commonly observed root-cracking that has been reported to occur in actual bridges [2] [15]. Large-scale testing presents itself as the most accurate representation of the fatigue behaviour expected to occur in an actual bridge at the price of complexity and cost of fabrication. The majority of large-scale experimental tests [11,13] carried experienced the reported higher propensity for root cracking, while there are examples of experiments that experienced toe-deck cracking [12].

2.2.2 List of Parameters of Influence

Factors that influence the fatigue performance of the OSDs include the deck geometry, weld geometry, wheel load transverse location, and weld defects, among other parameters. A literature review has been conducted to investigate the parameters of influence on the fatigue performance of OSDs.

2.2.3 Weld Geometry

The PJP weld used in the rib-to-deck joint can be considered the most influential parameter on the fatigue performance of OSDs, with improvement in fatigue performance as the level of weld penetration (LOP) increases. [1, 3, 4, 6, 8, 9, 11,12, 14, 16]. The proportional improvement of fatigue performance with

increasing LOP is only up to 75-80%, after which the fatigue life of an OSD will remain the same or slightly drop [12,13]. Furthermore, increasing the LOP beyond 80% increases the risk of weld defects during fabrication, such as welt melt-through and blow-through, which can severely degrade the fatigue life of a specimen.

Other aspects of weld geometry can also affect the fatigue life of OSDs, such as the presence of hot cracks [16] and the weld profile [15]. Hot cracks are shrinkage cracks that occur during the welding process when the liquid weld metal is insufficient to fill the voids between the solidifying weld metal. Hot cracks reduce the residual compressive stresses in the weld, which increases the likelihood of fatigue failure. Upon early discovery, hot cracks can be repaired relatively easily, outlining the importance of a thorough inspection of this defect. These cracks were the primary cause of extensive fatigue cracking in the Bronx- Whitestone Bridge in 66 of 408 deck panels [16].

A study suggests that the root size should be strictly controlled after comparing three different weld profiles: traditional single-sided weld seam, weld seam of large root and double-sided weld seam through numerical analysis [16]. The study concluded that the performance of the double-sided seam was significantly better than that of the traditional weld and that increasing the rib-deck inner seam distributes the stresses in a manner that is beneficial to the fatigue life and shifts fatigue failure to the weld toe rather than the root. The weld profile comparison also showed that a traditional weld seam performed better than a single seam with a large root.

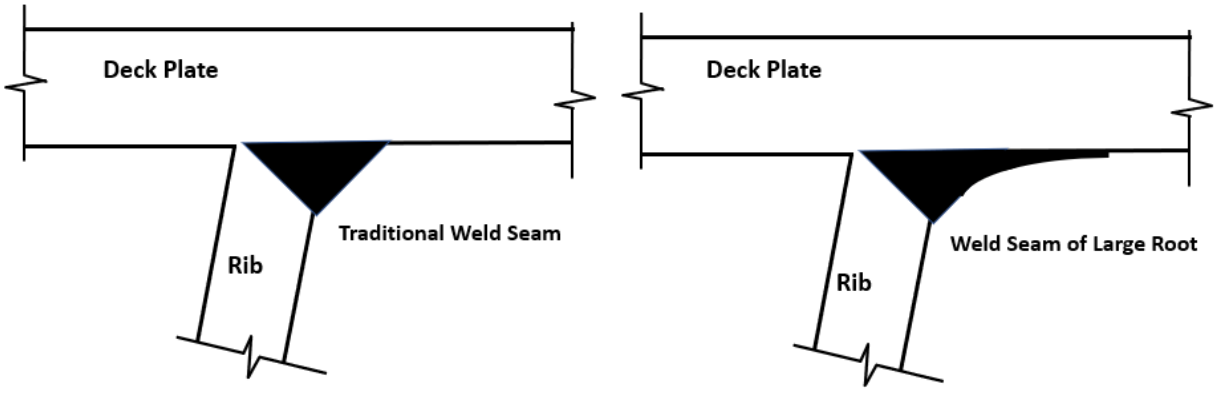

Figure 2.8: Illustration of Different Weld Profiles.

2.2.4 Deck Geometry

The deck geometry plays a major role in distributing the stresses from the wheel loads to the welds, thereby influencing the OSD's fatigue behaviour. Increasing deck plate thickness is the most beneficial parameter within the deck dimensioning on fatigue performance of OSDs the since the most reported forms of fatigue damage are cracks propagating from either the weld toe or rib through the deck plate [4, 12, 15]. Increasing the deck plate to 16mm seems optimal for fatigue performance, as it was quantified by [12] that increasing the thickness from 14mm to 16mm improved fatigue performance by 30%. In contrast, larger rib thicknesses have shown no effect [4, 17] on fatigue performance, while using larger overall ribs can be beneficial [4]. One study [18] showed that pre-cambering of decks improved the fatigue performance of the decks.

2.2.5 Transverse Loading Location

Two main numerical studies [9, 12] investigate the effect of the transverse load location on the stresses surrounding the rib-deck joint weld. One study evaluated the nature of the stresses at the ribs, membrane stresses, and deck plate stresses surrounding the weld. The load was placed at thirty varying transverse locations between the weld of interest and the two adjacent ribs. The results showed that the deck plate and membranes stresses were maximized when the load was on top of the weld, while stresses in the ribs were maximized when the load was on the adjacent rib [9]. The second study only investigated three scenarios which were: load was centred on the rib wall away from the analyzed weld (Load case 1), centred on the rib wall on top of the joint (Load case 2), and centred on the rib (Load case 3). The results showed that load cases 1 and two have the highest likelihood of developing cracks that propagate into the deck plate, while case 3 has a higher likelihood of developing a root-weld crack. The highest overall stress in the weld resulting from each case was load case 1, followed by 2 and 3 [12].

2.2.6 Fatigue Analysis Methods

FEA is a powerful tool that can be leveraged to provide fatigue life predictions using various techniques, each with its respective advantages and limitations depending on their application. The fatigue prediction of OSDs is commonly performed with the following approaches. 1. Hotspot Stress Approach 2. Notch Stress Approach 3. Linear Elastic Fracture Mechanics (see Figure 2.9). The hotspot stress and notch stress approaches are methods of determining the stress at the weld and then using established empirical curves from tests to determine the fatigue life based on the stress in the weld, such as S-N curves and FAT100. The LEFM approach does not require empirical curves, as the fatigue life is directly calculated by

evaluating the crack propagation rate through fracture mechanics [39]. The following subsection of this review will investigate the applicability and limitations of each of these approaches.

The hotspot stress method has been proposed in Eurocode-3 [40], fatigue design recommendations by the International Institute of Weld (IIW) [39] and JSSC for the fatigue assessment of welds supporting the technique's adequacy. Traditionally the Hotspot stress method has only been used to evaluate fatigue fillet welds at the toe. Research efforts have also shown that the notch stress approach presents itself as a viable solution for analyzing fillet welds of OSD rib-deck joints yielding conservative fatigue life estimates compared to the hotspot stress method when analyzing the weld toe. LEFM serves as a fatigue life prediction tool and can also be used to understand the fatigue cracking behaviour during crack initiation and propagation. However, LEFM is highly influenced by assumed crack properties, including direction, size, and modes which can lead to the complexity of the modelling procedure.

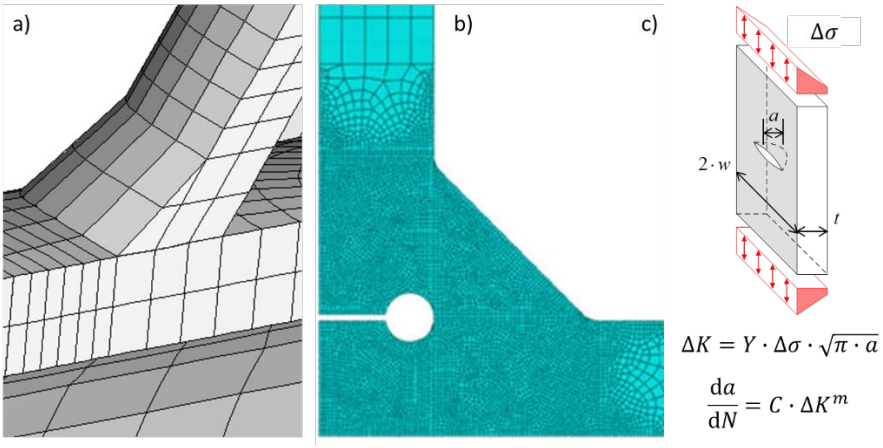

Figure 2.9: Three fatigue design methods – a) hotspot stress, b) notch stress, c) LEFM.

2.2.7 Hotspot Stress Method

In FE analysis, the weld stress of interest for fatigue design is usually found at the weld root or weld toe. These edge regions are sensitive to mesh size, meaning that the stress at those points increases towards infinity as the mesh size decreases. This poses a challenge in determining a characteristic design stress.The hot spot stress method overcomes this challenge by extrapolating the stress from reference points near the region of interest to obtain the nominal stress. The method is typically used to evaluate the structural stress the two of a fillet or full-penetration weld. Studies have shown that a practical limitation of this technique is it becomes less accurate when used to predict the stress at the weld root [1,5,12,39], which is the most commonly reported form of fatigue damage occurring in actual OSDs in bridges. The reason for this is that the weld root often represents a sharper change in geometry than the weld toe and can have a significant pre-existing crack-like defect present at the end of the fabrication process, before

fatigue loading even starts, if there is any lack of weld penetration. Note that the hotspot stress method is not limited to FE-based application and can also be used to predict the stress at the weld of an OSD experimentally by extrapolating the measured strains from nearby reference points [8] AASHTO recommends this method for the fatigue analysis of the weld toe of the rib-deck joints of OSDs in the absence of experimental data for a similar geometry to the OSD of interest.

2.2.8 Notch Stress Approach

The notch stress approach provides an alternative solution to obtaining the weld stress at a mesh-sensitive region of interest and accounting for the variation of the weld shape by replacing the stress contour at the weld with an effective one, as shown in the following image. An effective notch root radius of 1mm has yielded consistent results. The method can be used for fatigue life predictions at both the weld root and toe; however, it has been reported to yield better predictions in fatigue assessment of the weld root. The method has been deemed not applicable when a significant stress component parallel to the welds is limited to a weld thickness of 5mm or greater. Furthermore, a comparative analysis between the stress notch and hotspot stress approaches has shown that the hotspot stress approach is more reliable for fatigue predictions at the weld toes. The notch stress approach requires a very fine mesh which imposes the restrictions of only modelling a reduced local representation of the welds for feasible computational efficiency. [12, 17] implemented the stress notch approach to analyze the stresses at both the weld root and toe of rib-deck joints of OSDs.

2.2.9 Linear Elastic Fracture Mechanics (LEFM)

The fracture mechanics approach predicts fatigue life by calculating the crack propagation rate per loading cycle through the Paris-Erdogan crack growth law, which requires knowledge of the crack growth constants C and m, which can be obtained through literature or testing. Crack growth is proportional to an applied stress intensity factor (SIF) range, ΔK, which is a function of the crack size, stress range, and detail geometry. Theoretically, the LEFM approach can be applied without FE analysis. However, its often coupled with FE analysis to analyze complex geometries such as those present in OSDs. The SIF range calculation is highly dependent on the mode of cracking, which can be one of three types: 1) opening and closure of the cracks – Mode I, 2) in-plane shear – Mode II, or 3) out of plane shear – Mode III. For practical purposes, Mode I loading is often assumed to dominate and phase effects are conservatively ignored. This approach has been used to understand the propagation behaviour and provide practical fatigue life predictions for OSDs for root-to-deck plate cracks [20], Toe-deck plate cracks [21] and root-weld cracks [22].

2.2.10 North American Code Provisions on OSDs

Current CSA provisions from S6-19 as per Clause 10.16 require Design of OSDs to satisfy the requirements of clause 9.8.3 of AASHTO LRFD Bridge Design Specifications while still using loads and factors from CSA S6-19 for Serviceability (SLS), Fatigue (FLS), and Utlimate (ULS) Limit States. Due to the differnce in applied factors and loads, design scenarios may arrise where a certain design satisfies the imposed requirements when AASHTO provisions are implemented but not when CSA provisions are used. The purpose of this investigation is to quantify the impact of the differing loads and factors from both codes on a certain design's ability to meet imposed FLS requirements by obtaining key values that include stresses at the weld for a comparative analysis.

The total weight of the standard Canadian truck as per the CSA S6-19 is 625 kN while that of the American Truck is 320 kN.

A common challenge when analyzing OSDs is representing the stresses in critical regions surrounding the welds, which is paramount to the fatigue analysis of the connection. Fatigue analysis of the OSD welds was done by implementing Level 3 Design as per the AASHTO LRFD Specifications, which is the hotspot stress method. A comparison was done between the unfactored weld stresses resulting from both trucks and the factored stresses for finite and infinite fatigue life designs.

3 Experimental Program

This chapter summarizes the experimental program undertaken for the current thesis project, which investigated the fatigue performance of partial penetration FBG welds between aluminum HSS sections, as would commonly be used in applications such as pedestrian bridges.

3.1 Overview of program:

The experimental program conducted for this project consisted of 32 specimens that were divided into four groups with parameters varied in the experimental study including: HSS section size, corner radius, and post-weld surface grinding. Six identical samples were fabricated for each combination of parameters and tested at varying load ranges to generate an S-N curve for each specific geometry. Two specimens of each geometry group (8 of the total 32) were tested to find out the static strength of each geometry, while the remaining 24 specimens were fatigue tested to generate the SN-Curve. Determining the static strength of the specimen is necessary to identify a reasonable fatigue load range for the fatigue testing. The fatigue load ranges that were applied varied between 30% and 50% of the static strength.

3.2 Description of Specimen

The specimens consisted of welded aluminum HSS T-joints with properties summarized in Figure 3.1

Table 3.1. The dimensions in this table are defined in Figure 3.1

Table 3.1: Summary of dimension properties for each specimen group.

Sample Designation	Corner Radius (mm)	*L1* (mm)	*L2* (mm)	*W* (mm)	*t* (mm)
R-4.8	4.8	300	350	75	6.4
R-11.1	11.1	300	350	75	6.4
R-12.7	12.7	300	450	100	12.7
R-HG	N/A	300	650	100	12.7

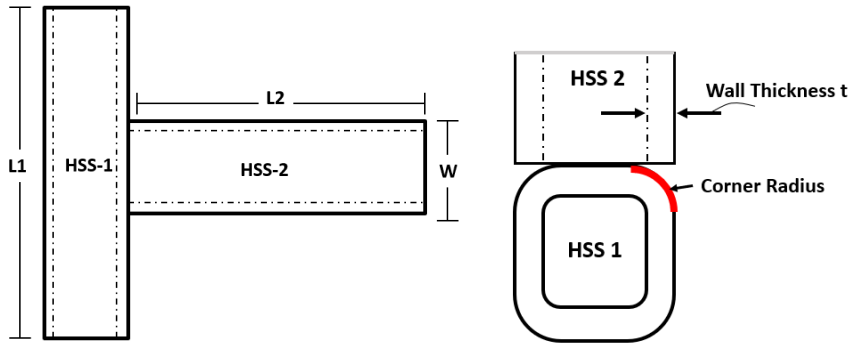

Figure 3.1: Specimen geometry and dimension definitions.

3.3 Description of Welding Process

Gas Metal Arc Welding (GMAW), also known as Metal Inert Gas (MIG) welding was employed in welding the aluminum T-joint flare bevel groove hollow structural sections investigated in this thesis. 5356 alloy electrode wire (filler metal) was used. GMAW is a welding process that utilizes a continuous wire electrode and a shielding gas to join metal components. The electrode wire is fed through a welding gun, while the shielding gas protects the weld from atmospheric contamination. The arc generates heat, melting both the wire and the base metal, which then solidify to form a weld joint.

3.4 Load Application and Test Accessories

All of the specimens were subjected to static or cyclic tensile axial loading. For the static tests, the load applied was monotonic (gradually increasing), while the load applied during the fatigue load was cyclic at tensile load ranges. Two different test frames were used, one for monotonic (static) testing and the second for cyclic testing, which both required plates to grip at each end, which were not provided with specimen geometry, thus introducing the need for geometric modification and the use of fixtures.

The top end of the HSS-2 member (see Figure 3.2) was thus fitted with a 9 mm thick gusset plate with varying dimensions W_p and L_p depending on the HSS member size (see Table 3.2). The plate was fitted by cutting out a portion of the HSS-2 member and fillet welding the plate with a weld length, d_p. The weld was overdesigned to ensure that is would not be the point of failure in the test.

Table 3.2: Summary of dimensions of fitted plates.

Sample Designation	Corner Radius (mm)	Lp (mm)	Wp (mm)	dp (mm)

R-4.8	4.8	300	150	150
R-11.1	11.1	300	150	150
R-12.7	12.7	500	200	250
R-HG	NA	400	200	200

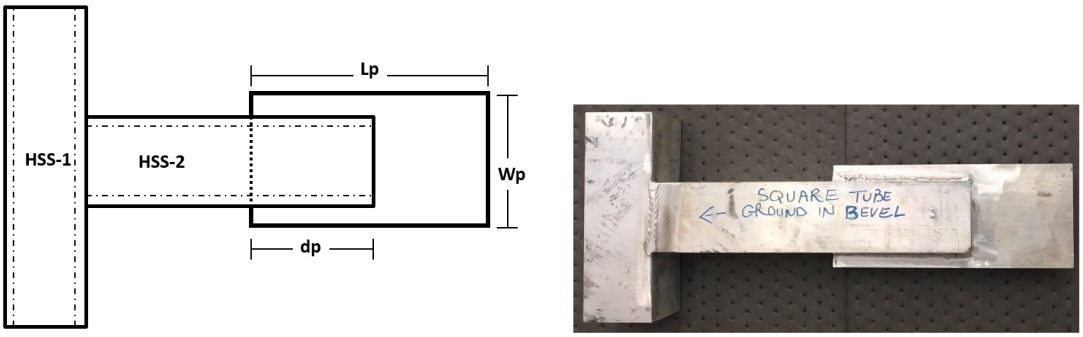

Figure 3.2: Diagram description of fitted plate dimensions.

The second end of the specimen was attached to the frame by placing the specimen on a square 100 mm × 100 mm × 400 mm steel fixture with a 20 mm plate welded to it, which could be gripped by the second end of the frame. The HSS-1 member was then attached to the steel fixture by passing a 60 mm × 60 mm × 400 mm steel bar inside the member and then connecting bar and the fixture with threaded rods, which passed through holes drilled near their ends. The edges of the steel bar were bevelled to prevent any localized damage from occurring on the bottom of the HSS01 member. The described fixture seemed to be efficient for the all the static and fatigue tests for the R4.8 and R11.1 groups.

Figure 3.3: Experimental setup of R4.8 specimen in Shorewestern Frame.

However, the steel bar that goes through the HSS-1 member did not have an adequate width for the larger R-HG and R-12.7 specimens. The inadequacy of the steel tube was discovered in the first fatigue test for a larger specimen (R-HG), which resulted in the propagation of a crack along the base of the HSS-1 member, which resulted into what resembles tear out failure after around 300,000 cycles.

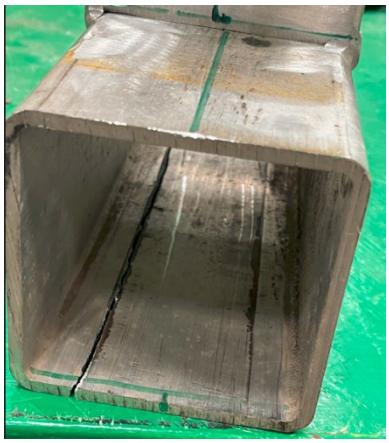

Figure 3.4: Tear out failure occurring in R-HG specimen due to undersized fixture bar.

To avoid this repetition of this undesired mode of failure, the steel bar was placed on top of a steel plate to further distribute the stress applied to the bottom of the HSS-1 member. The edges of the steel plate were beveled to minimize risk of stress concentrations from developing on the edge of the plate. The modified setup for the fatigue tests of the larger specimens is shown in Figure 3.5.

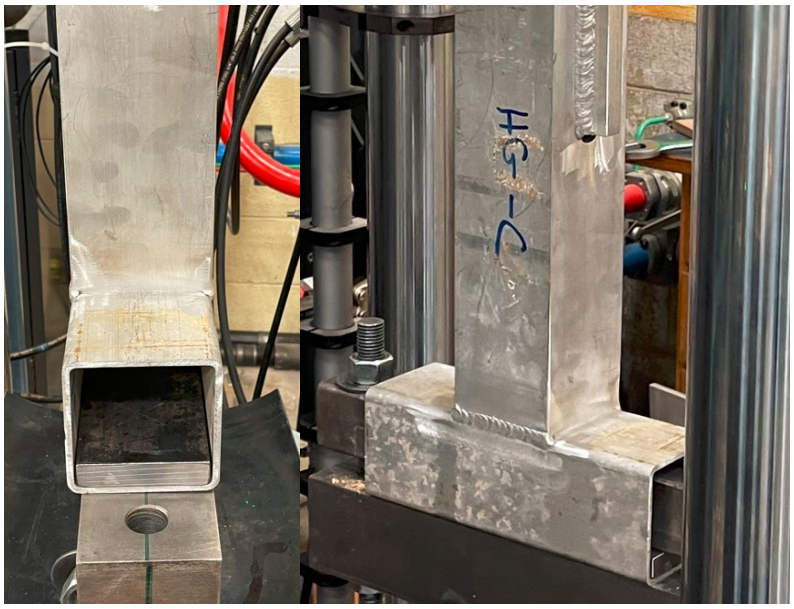

Figure 3.5: Modified experimental setup for larger specimens.

3.5 Static Tests

The static tests for this project were conducted by another researcher – Gerin Laurent [27] – with the purpose of obtaining the strength and ductility of these connections, which were later used by the author of this thesis to determine the appropriate stress range for fatigue testing for these specimens. The following subsection is a summary of the experimental setup and results of relevance to the fatigue tests that were carried out. Refer to [27] for a more detailed description of the static tests.

The tubular samples were tested statically in an MTS loading frame with a capacity of 600 kN (see Figure 3.6) using the fixture and gusset plate described in the previous section.

Figure 3.6: Experimental setup for static tests [27].

3.6 Effective Throat Measurement (static tests)

The effective throat throughout the weld length is not consistent, but a critical input for any strength calculation. To overcome this challenge, the method for measuring the effective throat for the static tests consisted of calculating the weld area from a scaled image of the weld fracture surface obtained after testing and dividing the weld area by the weld length to obtain the effective throat in mm.

To ensure consistency in obtaining the effective throat measurements for both the static and fatigue tests, the results obtained for the throat size for the specimens used in the static tests were checked by the author of this thesis. Both sets of results are tabulated in Table 3.3. Further description of the throat measurement process can be found in Section 3.10 of this thesis.

Figure 3.7: A failed tubular sample with weld area highlighted in red [27].

Table 3.3: Effective throat measurements carried out by Abdullah (author of this thesis) and Laurent [27].

ID	E (mm) Laurent	E (mm) Abdullah	Error (%)
R4.8-01	3.79	3.80	0.26
R4.8-02	3.55	3.59	1.15
R11.1-01	4.47	4.60	2.83
R11.1-02	4.35	4.54	4.48
R12.7-01	6.39	6.21	2.77
R12.7-02	5.99	6.08	1.53
HG-01	3.20	3.07	4.08
HG-02	3.03	2.99	1.34

The average error in the effective throat measurements when carried out by two different researchers was 2.3%, which was deemed acceptable for this research application. The error was calculated as:

$$\frac{\text{E (mm)Laurent} - \text{E (mm)Abdullah}}{\text{E (mm)Laurent}} \; x \; 100\% \tag{3.1}$$

The static test results reported in [27] are provided in Table 3.7, where the "measure throat area" is also taken from this reference.

Table 3.4: Summary of static test results.

Specimen Designation	Failure Stress (MPa)	Measured Throat Area (mm^2)	Failure Load (kN)
HG-01	179	650	116
HG-02	176	616	108
R4.8-01	183	578	106
R4.8-02	187	541	101
R11.1-01	195	682	133
R11.1-02	176	662	117
R12.7-01	168	1298	218
R12.7-02	180	1217	219

3.7 Fatigue Testing

The fatigue testing program consisted of 24 T-joint aluminum tubes designed to fail at the FBG welds. The specimens were subjected to cyclic tensile axial loading. The 24 specimens were categorized into

four geometric subgroups each with six specimens subjected to different load ranges at the same load ratio to obtain a representation of the fatigue life over different loading scenarios.

Table 3.5: Load parameters employed in fatigue tests for each specimen.

Test #	Specimen Designation	Static Failure Load (KN)	Max. Load (kN)	Min. Load (kN)	Test #	Specimen Designation	Static Failure Load (KN)	Max. Load (kN)	Min. Load (kN)
1	R4.8-A	103.5	30	6.0	**13**	R12.7-A	218.5	30	6.0
2	R4.8-B		33	6.5	**14**	R12.7-B		70	14.0
3	R4.8-C		35	7.0	**15**	R12.7-C		55	11.0
4	R4.8-D		40	8.0	**16**	R12.7-D		85	17.0
5	R4.8-E		43	8.5	**17**	R12.7-E		60	12.0
6	R4.8-F		45	9.0	**18**	R12.7-F		45	9.0
7	R11.1-A	124.8	30	6.0	**19**	HG-A	112.6	30	6.0
8	R11.1-B		33	6.5	**20**	HG-B		33	6.5
9	R11.1-C		33	6.5	**21**	HG-C		35	7.0
10	R11.1-D		40	8.0	**22**	HG-D		40	8.0
11	R11.1-E		45	9.0	**23**	HG-E		43	8.5
12	R11.1-F		43	8.5	**24**	HG-F		45	9.0

The fatigue load ranges varied between 30-45% of the average failure load obtained from the static (monotonic) strength test. Fatigue testing was conducted at a constant load ratio of 0.2. Table 3.5 summarizes the load parameters employed for each of the 24 fatigue tests.

3.8 Experimental Setup

The frame that was used for the fatigue testing was a Shore Western 1200 kN SC6000 frame. Figure 3.8 shows a specimen placed in the frame with the previously described fixture being used.

Figure 3.8: Experimental setup for fatigue tests.

3.9 Alignment of Specimen

Alignment of the specimens was considered to be a crucial factor when conducting the tests, as minor misalignment when loading the specimen would introduce bending stresses, which wouldn't have a significant effect on the static loading test results but would have a significant cumulative impact in high cycle fatigue performance. Misalignment can introduce nonuniformity in the stresses, which can influence the crack initiation location and growth direction – two crucial factors affecting the fatigue behaviour of the specimens. To ensure proper alignment during the tests, the following measure were taken:

- The steel fixture was machined after static testing to remove an observed offset of 0.5 mm and to make sure the fixture was perfectly square.
- Levelling tools were used prior to every test to ensure the specimens were vertically aligned.
- The fixture that was connected to the lower grip was left in the frame without being moved for the entire duration of the experimental program to avoid potential misalignment or change in alignment.
- Strain gauges were applied to two test specimens to compute at bending stresses that were applied on the tests to quantify if their effects were significant.

The strain gauges were placed on all four sides of the specimen and the strains recorded for each pair of parallel sides were compared. Upon investigation, the data from the strain gauges showed the bending effect of the tests did not exceed 0.8 MPa was deemed insignificant.

Figure 3.9: Placement of strain gauges for verification of specimen alignment.

3.10 Failure Displacements

The primary objective of this study was to investigate the fatigue performance of the welds, which required recording the following parameters:

- the number of cycles until failure,
- the crack initiation location, and
- the crack propagation direction.

Very restrictive displacement limits were imposed in controlling the actuator to capture the crack initiation and propagation in the specimens. Displacement limits for the smaller specimen were 0.5 mm to capture the crack propagation while 0.7 mm was used for the larger specimen. These values were established by incrementally increasing the displacement limits to find the optimum displacement limit for capturing the crack behaviour for the tested geometries. The number of cycles to complete failure was typically about 3%-10% more than the number of cycles for crack initiation. Therefore, it was decided that a specimen had failed when a crack was observable with the naked eye causing a displacement increase of 0.5 mm or 0.7 mm depending on the specimen size.

3.11 Modes of Failure for Fatigue Tests

Throughout the 24 fatigue tests, four different results were observed: fatigue failure in the weld, fatigue failure in the heat affected zone (HAZ), fatigue test runouts (no failure), and premature fatigue failure due to set-up complications.

Failure in the weld: This is the desired failure mode for this experimental program as it gives insight into fatigue cracking mechanism and generates data points that can be used to define a design curve. The observed fatigue failures in the weld were typically characterized by a crack that initiated and then propagated from one side of the weld to the other as shown in Figure 3.10.

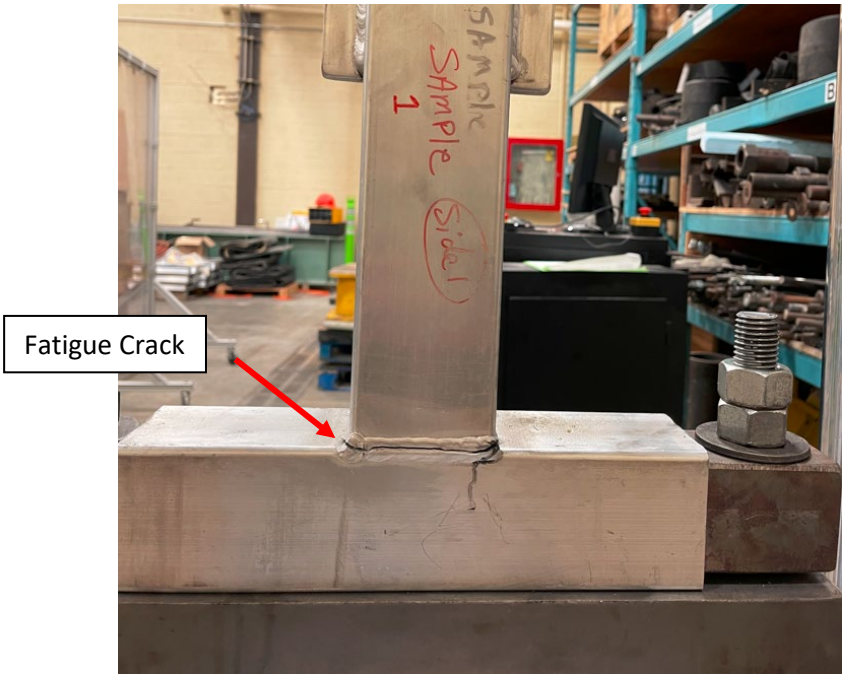

Figure 3.10: Fatigue cracking in the weld of an R4.8 sample.

Failure in the heat affected zone: The heat due to welding reduces the strength of the aluminum surrounding the weld in a region referred to as the heat affected zone (HAZ). Typically, the strength reduction can vary between 30%-50%. However, there is variability associated with material behaviour and also the welding process, and the effect of head due to welding on the fatigue performance is less certain. A single specimen experienced this failure mode after 2.1×10^6 cycles.

Fatigue test runout: This occurs when the number of cycles reaches a number that is sufficiently large that the test is stopped and the fatigue life is considered to be infinite for practical purposes. In the current study, 4 million cycles was the arbitrary threshold at which the tests were stopped in this way. Two specimens from the R12.7 group were classified as “runouts” in this test program.

Premature failure: One specimen failed due to tear-out in the bottom HSS member as described in the load applications and fixtures discussion in Section 3.3. Another specimen failed at the start of testing due to complications that arose when calibrating the Shore Western SC6000 frame, resulting in instantaneous failure prior to fatigue loading and therefor an unusable test result.

Figure 3.11: Fatigue cracking in the heat affected zone of an R-HG sample.

3.12 Effective Throat Measurement (Fatigue Tests)

As mentioned earlier, a critical parameter when analyzing structural performance is the effective throat, because it is the parameter used to calculate the cross-section area of the weld and afterwards the stress that is applied to the specimens. Two methods were used to calculate this parameter in the current study: 1) measuring the failure surface of the weld, and 2) using code recommendations from the AISC (American International Steel Construction) [41]. The measurement was done by taking an image of the failure surface with a phone camera but with the use of alignment tools to make sure the surface of the lens was parallel to the failure surface of the weld with the lens coinciding with centroid of the HSS section. The images were then imported into AutoCAD and the weld area was calculated by tracing with the software and then calculated using another software feature. The effective throat of the weld is afterwards calculated by dividing the area obtained by the length of the weld. The following image is an example of the failure surface image that was used to calculate the effective throat of the weld. This process essentially follows the one employed in [27], but with each step performed “manually”.

Figure 3.12: Specimens failed in fatigue showing region of weld where effective throat was measured by calculating area surrounded by white lines.

The second method is meant for determining the throat in applications where the effective throat of the weld cannot be determined or is unknown, such as in design of a weld for future fabrication. The AISC recommends using a throat of 5/8 the corner radius of the HSS member in this case. The resulting throat dimensions are reported in Table 3.7

3.13 Experimental Results

The 24 fatigue tested specimens were not all included in the fatigue analysis of the tubes because of complications that occurred in the lab, fatigue runout, and failure occurring not in the weld the following is a summary of the tests and their respective modes of failure:

- two specimens were “runouts”
- one specimen failed due to errors in calibrating the loading frame, and
- one specimen failed by tear-out of the bottom of HSS due to the use of a small size steel fixture bar, which caused additional bending in the tube wall.

The statistical analysis of the fatigue performance of the investigated FBG welds performed for this study was solely based on the results obtained from the remaining 20 tests. The test results are summarized in Table 3.6. with tabulated stress values based on effective throat measurements that were done by the author of this report.

Table 3.6: Fatigue test results.

Test #	Specimen Designation	Load Range (KN)	Stress Range (MPa)	Number of Cycles to Failure
1	R4.8-A	30.0-6.0	38.5-7.7	1,714,813
2	R4.8-B	32.5-6.5	38.6-7.7	504,080
3	R4.8-C	35.0-7.0	52.6-10.5	118,915
4	R4.8-D	40.0-8.0	49.6-9.9	127,104
5	R4.8-E	42.5-8.5	-	Equipment error
6	R4.8-F	45.0-9.0	60.6-12.1	100,923
7	R11.1-A	30-6	38-7.6	369,606
8	R11.1-B	32.5-6.5	35.5-7.1	288,776
9	R11.1-C	35-7	37.49-7.2	526,865
10	R11.1-D	40-8	36-7.2	1,081,948
11	R11.1-E	42.5-8.5	45.8-9.2	218,409
12	R11.1-F	45-9	42.6-8.5	415,731
13	R12.7-A	30-7	25.8-5.2	Runout
14	R12.7-B	70-14	42.8-8.6	140,867
15	R12.7-C	55-11	43.9-8.8	533,290
16	R12.7-D	85-17	60.4-12.1	57,731
17	R12.7-E	60-12	36.5-7.3	683,932
18	R12.7-F	45-9	38.7-7.7	Runout
19	HG-A	30-6	38.5-7.7	Tearout Failure
20	HG-B	32.5-6.5	21.3-4.3	2,349,457
21	HG-C	35-7	44.9-9	Runout
22	HG-D	40-8	26.6-5.3	1,789,484
23	HG-E	42.5-8.5	21.5-4.3	2,644,338
24	HG-F	45-9	30.6-6.1	759,471

3.14 Effect of Varied Parameters on Fatigue Performance

In Figure 3.13, the test results are plotted on a log-log stress-life (S-N) plot with the detail categories used by the Aluminum Design Manual [30] and CSA S157 [29] and S6 [23] plotted for comparison purposes. From a quick inspection, it can be seen that the HSS member size and grinding of the tube corners did not seem to have influential effects on the results. The scatter in the results indicates that the main parameter of influence on the performance of a specimen was the level of stress in the weld, which is primarily a function of the effective throat. The size of the effective throat is dictated primarily by the corner radius of the HSS member, and the larger the corner radius, the larger the area of the partial penetration weld, which will in turn lead to a reduction the stress applied to the weld for a given load level.

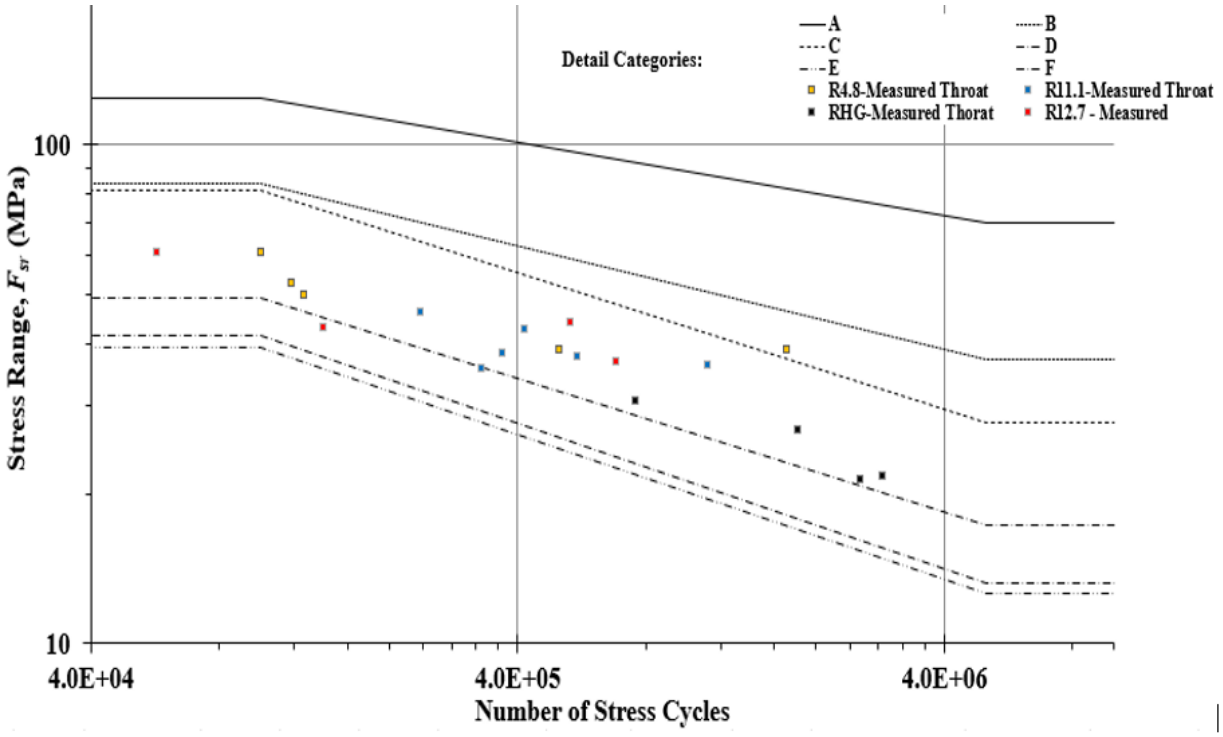

Figure 3.13: Test results (area used to calculate the stress based on measured effective throat).

3.15 Statistical Analysis of Test Results

When analyzing the results of fatigue tests for the purpose of generating a design S-N curve, a line of best fit must first be generated to describe the trend of this data. The line of best fit is afterwards used to generate a design curve, which guarantees a predetermined survival probability (95% is used in most international standards or 97.7% - two standard deviations below the mean – in the North American standards for the fatigue design of aluminum structures). The design curve will afterwards be used to

relate the fatigue performance of the welded configuration to one of the standard detail categories. The statistical analysis that was used to generate the line of best fit and design curve was the guideline for analysis of fatigue data published by the International Institute of Welding (IIW) [42].

The relationship between the number of cycles (N) and stress range is assumed to be exponential:

$$N = C\Delta\sigma^m \tag{3.2}$$

The linearization of this equation yields the following equation:

$$\log N = \log C - m \log \Delta\sigma \tag{3.3}$$

The line of best fit is afterwards generated using least squares regression to obtain C and m. based on the IIW recommendations, the design curve that can be directly used by engineers to evaluate the fatigue performance of connection must ensure a survival probability of 95% at a level of confidence in the mean of 75%. To obtain the design curve from the line of best fit characteristic values of C and m should be obtained. The IIW method for obtaining the design curve calculates the value of C corresponding to the required survival probability while assuming that the slope m is constant:

$$\log C_i = \log N_i + m \log \Delta\sigma_i \tag{3.4}$$

The next step is to calculate the standard deviation, σ, for $(\log C)_m$. Lastly the required characteristic value to obtain the survival probability can be calculated through the following equation where k is a factor that considers the effect of the sample size on the variance of data:

$$\log C = (\log C)_m - k \times \sigma' \tag{3.5}$$

The IIW requires a sample size of 10 or more for this analysis to be valid and the larger the sample size the smaller of k up to as point at which a large increase of the sample size will result in an insignificant decrease in k which roughly around 100 samples the corresponding k is 1.9. The corresponding k for 20 samples is 2.32.

As shown in Figure 3.14, the result of this exercise for the tests conducted in this study is a design curve associated with a 95% survival probability falling very close to the Category E design curve. This means that if an engineer wants to easily analyze the fatigue performance of PJP FBG welds for aluminum T-joints or similar structural configurations, the engineer should simply refer to the Category E S-N curve and locate the stress range corresponding to the desired fatigue life.

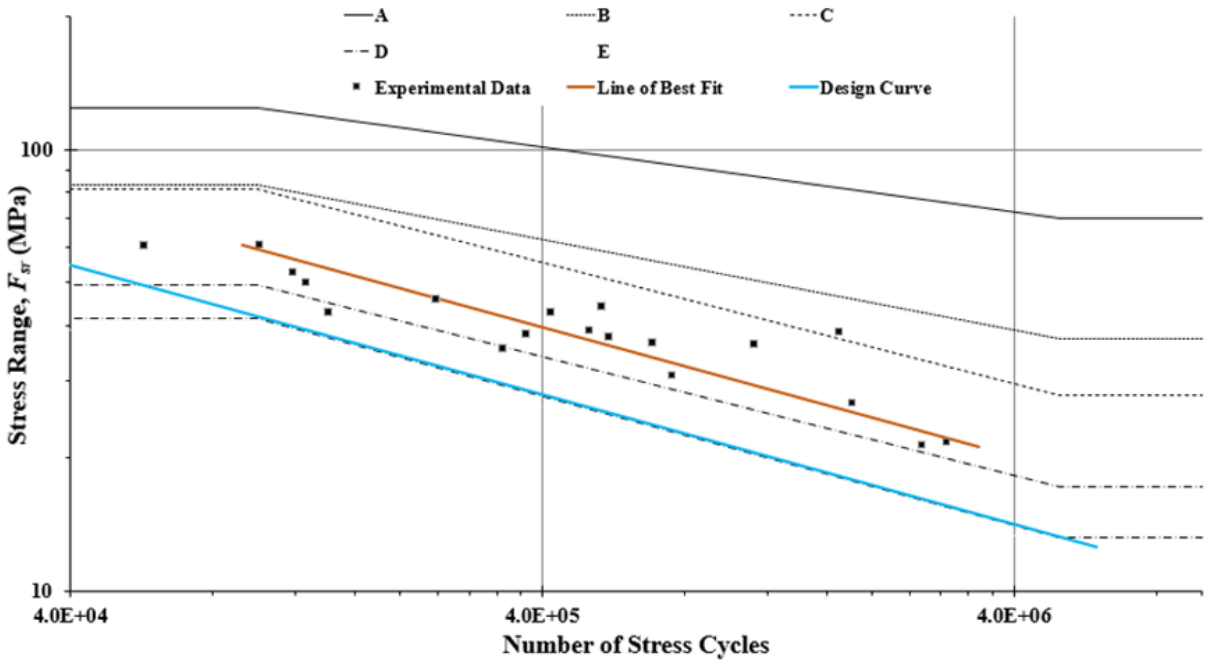

Figure 3.14: Statistical analysis of fatigue tests (stress based on measured throat).

3.16 Effective Throat

In the event that the actual throat thickness of a partial joint penetration weld is unavailable (as would typically be the case in a new design), code recommendations can be used to assume an effective throat as a fraction of the corner radius. The AISC (American Institute of Steel Construction) 360-16 code [41] recommended throat of 5/8^{ths} of the corner radius. A statistical analysis generated using the code-based throat is plotted in Figure 3.15 and shows a much higher scatter in the test data. Note that the results from the hand ground specimens were excluded from this portion of the study because the corner radii varied along the length of the weld considerably. Due to the higher scatter of the plotted results, a value for the slope, *m*, of the S-N curve had to be assumed. For this purpose, the slope of the Category E design curve was used. Although the line of best fit through the test results based on the code-assumed throat was relatively close to that of the measured throat, the larger scatter resulted in a higher standard deviation, which in turn shifted the design curve far below Category E.

Since there is no detail category below Category E, a practical solution would be to recommend a different effective throat for fatigue design purposes. By trial and error, it was found that an effective throat of 3/8^{ths} of the corner radius resulted in an upward shift of the calculated design curve, so that it falls roughly on top of the Category E curve, as shown in Figure 3.16.

Table 3.7: Measured (MT), AISC Code Throat (CT), Recommended Throat (RT) and comparison of weld throats.

Test #	Specimen Designation	Measured Throat (MT) (mm)	AISC Code Throat (CT) (mm)	Recommended Throat (RT) (mm)	CT/MT (%)	RT/MT (%)	RT/CT (%)
1	R4.8-A	4.35	3	1.8	69%	41%	60%
2	R4.8-B	3.76	3	1.8	80%	48%	
3	R4.8-C	4.08	3	1.8	74%	44%	
4	R4.8-D	3.67	3	1.8	82%	49%	
5	R4.8-E	4.46	3	1.8	67%	40%	
6	R4.8-F	4.70	3	1.8	64%	38%	
7	R11.1-A	4.41	6.94	4.16	157%	94%	
8	R11.1-B	5.14	6.94	4.16	135%	81%	
9	R11.1-C	4.62	6.94	4.16	150%	90%	
10	R11.1-D	5.92	6.94	4.16	117%	70%	
11	R11.1-E	5.24	6.94	4.16	132%	79%	
12	R11.1-F	5.32	6.94	4.16	130%	78%	
13	R12.7-A	-	7.94	4.76	-	-	
14	R12.7-B	8.73	7.94	4.76	91%	55%	
15	R12.7-C	6.68	7.94	4.76	119%	71%	
16	R12.7-D	7.50	7.94	4.76	106%	64%	
17	R12.7-E	8.76	7.94	4.76	91%	54%	
18	R12.7-F	-	7.94	4.76	-	-	
Average % Difference					104%	62%	60%
19	HG-A	-					
20	HG-B	6.115					
21	HG-C	-					
22	HG-D	6.01					
23	HG-E	7.89					
24	HG-F	5.89					

The analysis reveals that the average ratio of the code-based throat to the measured throat is 104%, with a standard deviation of 0.31, indicating an accurate estimation of the weld throat but with a relatively large scatter. Upon plotting the resulting stresses corresponding to the code-based throat, the design curve drops significantly below the obtained detail category E due to the scatter of the throat dimensions. However, reducing the code-based throat from 5/8ths the corner radius to 3/8ths the corner radius results in an underestimation of the average effective throat by 38%. Nevertheless, the resulting stresses produce a

design curve that is in agreement with the test data (Category E). Note that no code-based throat nor recommended throats are provided in Table 3.7 for the R-HG specimens because each specimen has varying corner radius along its radius.

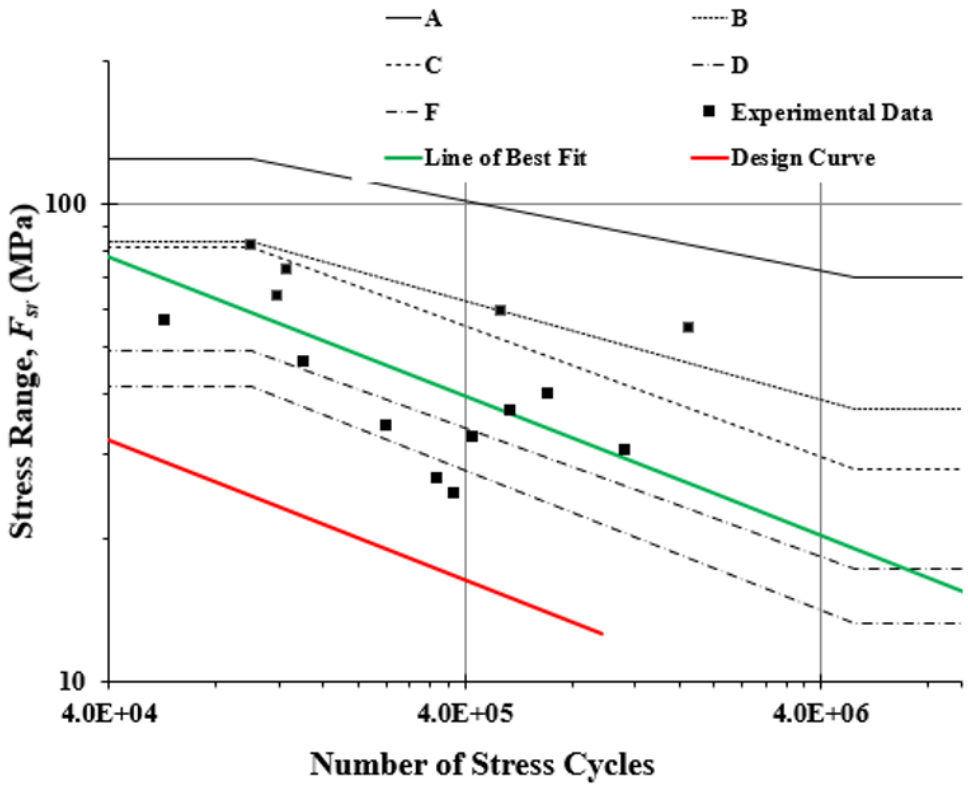

Figure 3.15:SN curve with stress calculated based on area obtained from AISC recommended throat.

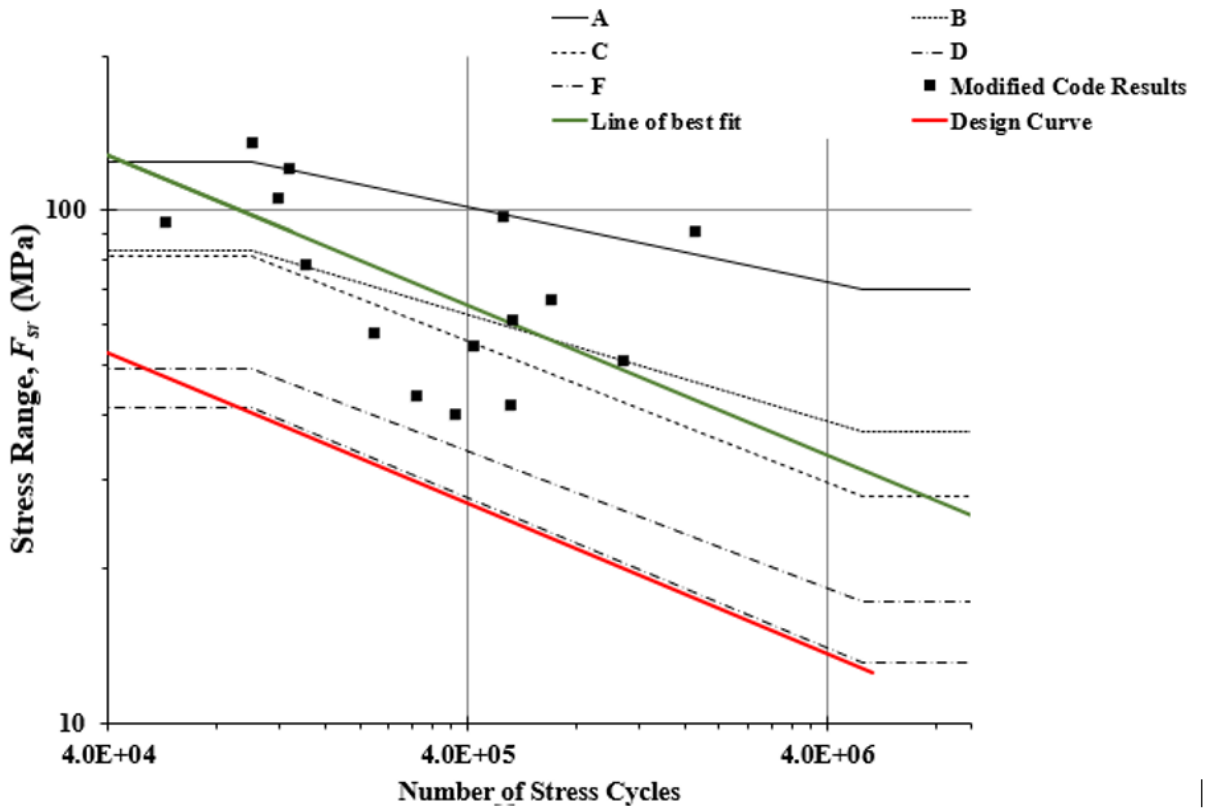

Figure 3.16: SN curve with stress calculated based on area obtained from proposed throat.

4 Analysis of Results

This chapter summarizes an analysis of the partial penetration FBG weld tests presented in Chapter 3 using linear elastic fracture mechanics (LEFM). In the following sections, the theory and tools used to conduct this analysis are first reviewed. Results of the analysis are then presented.

4.1 Revisiting Linear Elastic Fracture Mechanics (LEFM)

Linear elastic fracture mechanics (LEFM) provides a mathematical approach for the prediction of crack growth and fracture in materials subjected to fatigue loading. The approach is based on the concept of a stress intensity factor (SIF), which describes the intensity of the stress at the tip of a crack. The SIF is used to calculate the rate of crack growth, which can be related to the number of cycles to fracture. This approach is advantageous because it does not rely on the use of empirical S-N curves.

LEFM has been widely used in engineering applications, particularly in the fatigue analysis of structural elements in bridges, aircraft, and pressure vessels, where the presence of cracks can lead to failure.

In this approach, the material is assumed to be linearly elastic. This assumption is particularly valid for metals, such as aluminum or steel, under the low-cycle fatigue regime.

Cracks can propagate in three modes (see Figure 4.1), each with its own characteristic stress intensity factor (SIF). Mode I cracking typically dominates. The SIF is a critical parameter that determines the stability of a crack and is used to predict when a crack will grow and how quickly.

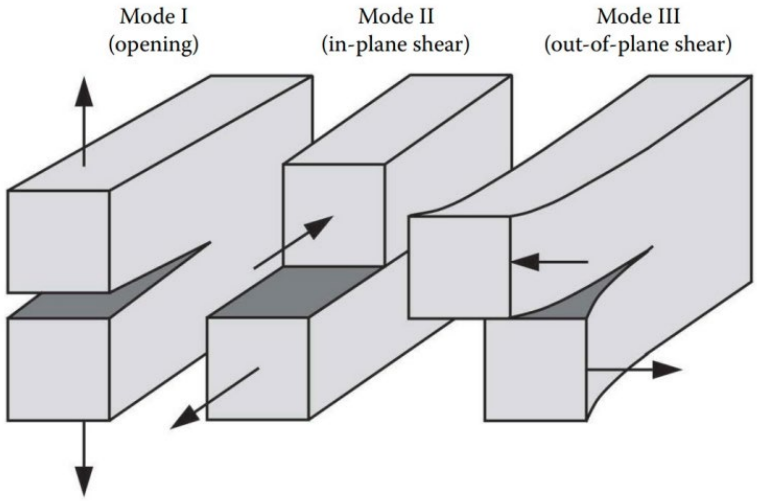

Figure 4.1: Modes of Cracking of LEFM [27].

4.2 Paris' Law

Paris' law relates the crack growth rate to the stress intensity factor (SIF). Paris' law (sometimes referred to as the Paris-Erdogan crack growth law) was first developed by P.C. Paris and F. Erdogan in 1963, and it has been widely used to predict the rate of crack growth in structures under various loading conditions. The relationship between the crack growth rate and the SIF provides a means of predicting the progression of a crack over time. However, it is important to note that the law is only valid for small crack growth rates and for materials operating in the linear-elastic domain. It states that the crack growth rate, da/dN_f, is proportional to the SIF range raised to a power, m. The relationship is expressed as:

$$\frac{da}{dNf} = C \cdot \Delta K^m \tag{4.1}$$

where C and m are Paris's law constants and are obtained from literature on applications concerning fatigue of aluminum under similar loading circumstances [39].

Upon integrating the term in equation 4.1, the fatigue life N_f can be equated to

$$N_f = \int_{a_o}^{a_f} \frac{da}{C_0 \left(\Delta K_{eff}^m - \Delta K_{th}^m\right)} \tag{4.2}$$

where:

a_f is the crack size that causes failure and is calculated as:

$$a_f = \frac{t}{2}\left(1 - \frac{\rho_o \, \Delta\sigma_n}{\sigma_u(1-R)}\right) \tag{4.3}$$

ρ_o is the degree of penetration and t is the thickness of the material.

a_o is the initial crack size calculated as:

$$a_o = t(1 - \rho_o) \tag{4.4}$$

ΔK_{th} is the threshold value for the SIF range that separates the crack initiation and crack propagation regimes. Geometric and loading conditions that result in a ΔK_{eff} that is less than ΔK_{th} will cause no crack propagation. ΔK_{th} is a material dependent property that can either be obtained experimentally through conducting a crack propagation tests or through literature. For this study, the ΔK_{th} used for aluminum is obtained from the IIW Recommendations [42] and can be calculated as:

$$\Delta K_{th} = 56.7 - 72.3R \geq 21 \tag{4.5}$$

If the load ratio, *R*, is equal to 0.2 as it was for the tests presented in Chapter 3, then:

$$\Delta K_{th} = 42.24 \text{ MPa}\sqrt{\text{mm}}$$

ΔK_{eff} is the effective stress intensity range calculated by multiplying the difference between the stress intensity factors resulting from the maximum K_{Max} and minimum loads K_{Min} applied in each load cycle with a factor, *U*, that accounts for crack closure effects. The resulting equation takes the form:

$$\Delta K_{eff} = (K_{Max} - K_{Min}) \cdot U \tag{4.6}$$

Crack closure refers to the phenomenon in which crack opening is partially delayed by the interaction between the crack faces and the surrounding material. This interaction can result in reduction of the stress intensity factor (SIF) at the crack tip. Plastic deformation of the material near the crack tip can result in partial closure of the crack even when it is subjected to tensile loading. Consideration of crack closure results in more realistic representation of the crack behaviour while yielding a less conservative fatigue life prediction. Various methods exist to model crack closure, including yield strip models and simple linear relationships. However, a method was proposed by Newman et al. [43] mathematically relating stress to the clack closure factor *U* and then modified by Mclung [44] by replacing the stress terms in the equations with stress intensity factor terms. The modified method proposed by Mclung has been chosen for this study because it has been successfully used to analyze cracking in aluminum welds [27].

The equation used to calculate *U* takes the form:

$$U = \frac{1 - \frac{K_{op}}{K_{Max}}}{1 - R} \tag{4.7}$$

$$\frac{K_{op}}{K_{Max}} = C_0 + C_1 R + C_2 R^2 + C_3 R^3 \tag{4.8}$$

where:

$$C_0 = (0.825 - 0.34\alpha + 0.05\alpha^2)(\cos\left(\frac{\pi}{2} \cdot \frac{K_{Max}}{K_o}\right)^{\frac{1}{\alpha}} \tag{4.9}$$

$$C_1 = (0.415 - 0.071\alpha) \tag{4.10}$$

$$C_2 = 1 - C_0 - C_1 - C_3 \tag{4.11}$$

$$C_3 = 2C_0 + C_1 - 1 \tag{4.12}$$

K_{op} is the SIF caused by the opening stress σ_{op} that will result in crack opening when considering the crack closure effect, which is a function of the stress ratio and K_{max}.

α is equal to 1 or 3 for plain stress or plain strain conditions respectively.

K_o is the flow stress intensity factor which can be calculated by

$$K_o = \sigma_o\sqrt{\pi a} \tag{4.13}$$

where a is the crack size and σ_o is the flow stress (average of the yield and ultimate stresses).

4.3 J-Integral

The J-integral method is a path-independent and a global approach to fracture analysis, which provides a means to finding the stress intensity factor that can be robustly coupled with finite element analysis to obtain the SIF for complex geometries. It provides a means of calculating the energy release rate, which is a measure of the energy required to propagate a crack.

The J-integral is defined as the work done by the external load on a crack-containing body, and it is given by the following equation:

$$J = \int K\, dA \tag{4.14}$$

where K is the stress intensity factor along the crack, and dA is the incremental area around the crack. The J-integral is calculated by integrating the stress intensity factor along a closed contour surrounding the crack, and it provides a measure of the energy available to drive the crack growth.

The J-integral method has several advantages including its ability to consider the effects of stress and deformation around the entire crack, its path independence, and its applications in the presence of crack closure. These advantages make the J-integral method a valuable tool in the analysis of cracks in structures, particularly for structures complex geometries such as partial penetration FBG welds, where the effects of crack closure and stress redistribution cannot be neglected.

For linear elastic conditions and Mode 1 cracking, the relationship between the energy release rate and the stress intensity factor can simplified as follows, where v is Poisson's ratio, which was taken as 0.33, and E is the modulus of elasticity of aluminum ,which was taken as 70 GPa:

$$J = K^2 \cdot \left(\frac{1-v^2}{E}\right) \tag{4.15}$$

The fatigue life of a certain geometry can be predicted numerically through the analytical process of mathematically quantifying the crack propagation rate through linear elastic fracture mechanics (LEFM).

However, when working with complex geometries it is often coupled with finite element modelling to find a solution where a closed-from SIF solution does not exist. Throughout this presented methodology, a simplified 2D model of the initial cracking behaviour of the specimen was used to obtain the SIF using established LEFM equations. The limitations of the simplified model will be discussed. Afterwards, a complex 3D model will be used for the analysis to compare the stress surrounding the weld from both 2D and 3D models and calculate the fatigue life of the specimen using the J-integral method.

4.4 2D Representation of Test Specimen

The objective of the 2D modelling representation was to validate the J-integral approach for this geometry and loading conditions by comparing the result obtained from a finite element model implementing the J-integral approach with calculations for the SIF with an established closed form solution for a single edge crack. The simplified analysis is limited to a single cross section at the middle of the tubes that represents of a single side of the walls of both HSS members, and the welded material as shown in Figure 4.2

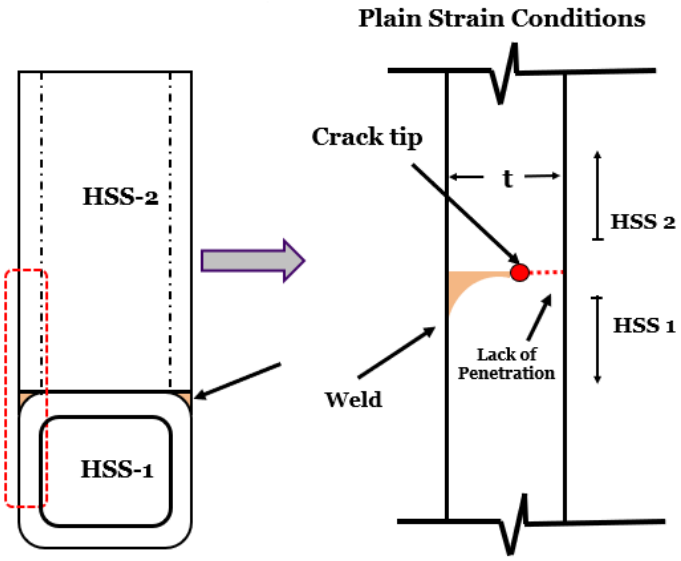

Figure 4.2: Simplification of 3D behavior of the tubes (shown on the left) to only consider the behavior of the walls of the tube for a 2D reduction (shown on the right)

If the assumption is made that that single cross section has a thickness going into the page that is infinite (2D plain strain behaviour), then the earlier-mentioned simplification is obtained. This simplification assumes that the top and bottom walls of HSS-1 have no effect on the model and that the fatigue life of the specimen can be represented by the stress behaviour at the middle region of the HSS along its thickness ("into the page" with reference to Figure 4.2

A crack initiation point, and direction must be assumed to conduct the LEFM analysis. The crack initiation point is likely to occur in a region that has a stress concentration due to geometric irregularity or from a point where residual stresses are high, which are both characteristics of welds. The crack that would cause fatigue failure was assumed to propagate from the inside out because the lack of penetration results in a "crack-like" defect with a particularly high SIF at the tip. This simplification can be particularly useful as it can be directly compared to a single edge cracked plate LEFM problem as shown in the following image.

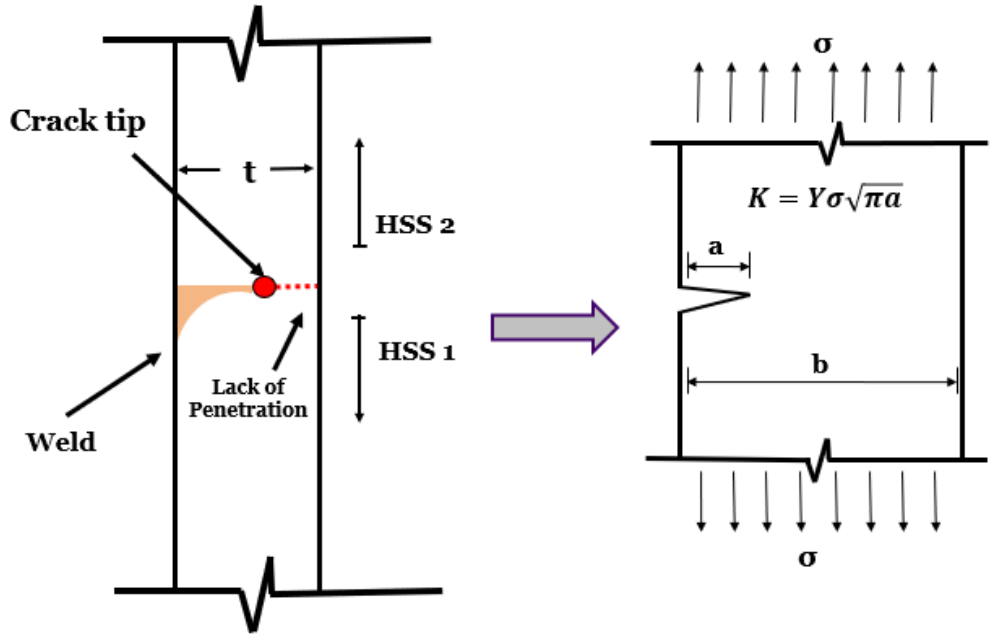

Figure 4.3: Comparison between 2D representation of welded HSS walls with theoretical edge crack.

4.5 Hand Calculation of SIF for Simplified 2D Model

The analyzed case is for crack initiation during a single load cycle from an unstressed state to a maximum stress of 46.88 MPa, which results from a load of 22.5 kN. The SIF for a plate with a thickness *b* and a single edge crack with a crack thickness *a* can be found through the following expression:

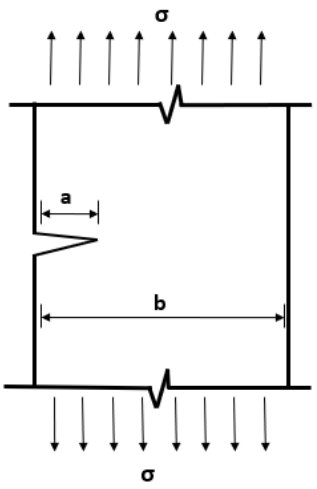

Figure 4.4: Axial stress applied on a cracked 2D solid with crack width a and a thickness b

$$K = Y \cdot \sigma \cdot \sqrt{\pi a} \tag{4.16}$$

where σ is the net section stress applied, Y is a correction factor, and a is the crack size.

The correction factor for this problem changes as the crack size grows and can be calculated as:

$$Y = 1.12 - 0.234\left(\frac{a}{b}\right) + 10.55\left(\frac{a}{b}\right)^2 - 21.72\left(\frac{a}{b}\right)^3 + 30.39\left(\frac{a}{b}\right)^4 \tag{4.17}$$

The thickness b is for the analyzed case is the wall thickness of 6.4 mm and the crack size a of 3.2 mm, which corresponds to the weld seam resulting from a 50% PJP weld. By substituting the relevant values into Equations 4.16 and 4.17, we can determine the following resulting stress intensity factor (SIF) and energy release rate:

$$K = 420.07\ MPa\sqrt{mm} \rightarrow J = 2.246\frac{Joules}{mm^2} \tag{4.18}$$

4.6 2D FE Model Description and Validation

The geometry of the model was a rectangle with a seam with 3.2 mm thickness representing the unwelded portion between the walls for 50% PJP weld as shown in Figure 4.5. In this figure, the thickness of the HSS-1 and HSS-2 members is 6.4 mm, and their lengths are 300 mm.

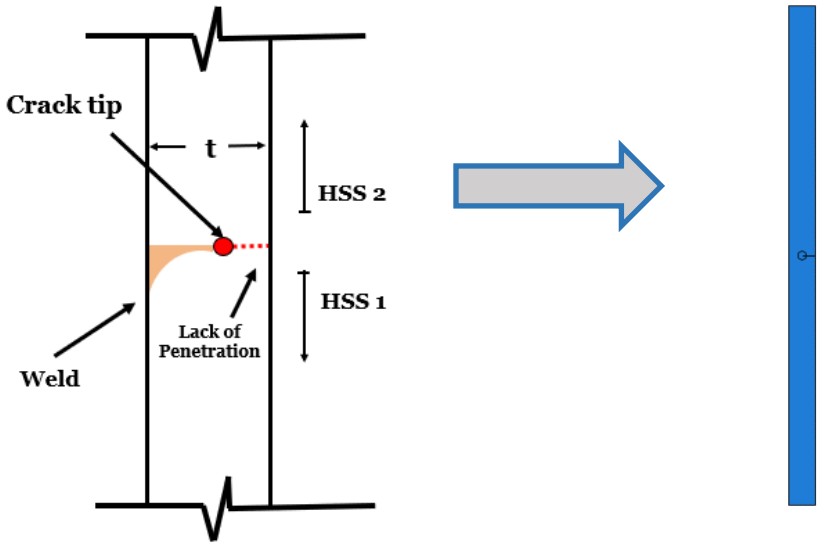

Figure 4.5: 2D plain strain model of HSS walls welded together with lack of penetration to compute J-integral.

A lack of penetration or "crack" is defined at the tip of the seam, which is within the HSS wall with a crack propagation direction outwards (to the left). Note that throughout the analysis the actual curved shape of the weld is not considered to maintain to model's simplicity and robustness.

A load if 22.5 kN was applied at the midpoint of the tops surface of the model and fixed boundary conditions were applied to the bottom surface to restrict any unwanted movement.

The mesh consisted of CPE8R elements in ABAQUS 2D ,which are plain strain elements with second-order quadrilateral reduced-integration. The mesh size is somewhat consistent throughout the entire model with a reduction in size in the region surrounding the crack tip as the J-integral approximation is mesh sensitive. A region surrounding the crack tip is defined as the plasticity zone where the mesh becomes circular to take the shape of the contours and increasingly fine to ensure convergence for J-integral solution. The plasticity zone is a circle with the radius of

The size of the plasticity zone was determined based on *K* resulting from a load which is 45% of the static load at 10% of the wall thickness. Which results in the size of a plasticity zone if 0.75 mm. The size of the plasticity zone that was chosen was 3 mm for all the models that were used.

$$r_p = \frac{1}{3\pi} \cdot \left(\frac{K}{\sigma_y}\right)^2 \tag{4.19}$$

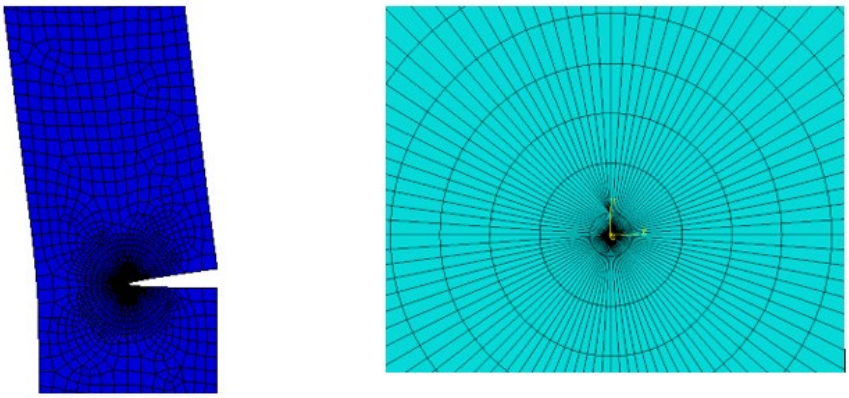

Figure 4.6: Deformed shape of 2D model (left) and ABAQUS 2D plain strain model Showing mesh surrounding crack tip of model within the plasticity zone (right).

The results of the J-integral calculations at four separate contours varied between 2.514 to 2.526, which was deemed as an acceptable level of error with respect to the closed form solution (0.48%). The result obtained when averaging the energy release rate across the contours was the following:

$$K = 420.6\ MPa\sqrt{mm} \rightarrow J = 2.252\ \frac{Joules}{mm^2}$$

The result serves as a validation that the J-integral approach is being implemented correctly and shows that the J-integral approach is appropriate for LEFM analysis of the FBG welds. However, this simplification does not account for the complex geometry of the tubes, particularly the top plate of the HSS-1 member and the flanges of the HSS-2 member adjacent to the weld. Accounting for the components neglected in the 2D analysis will result in an increase in stiffness in the connection, which will cause a redistribution of the weld stresses, which requires a 3D model to capture.

4.7 3D FE Model Description

The objective of this portion of the study was to use LEFM as a tool for predicting the fatigue life of the aluminum T-joints and for a comprehensive analysis of the crack behaviour of the tubes. Multiple 3D models of the tubular joints associated with 10% increments of weld penetration were constructed to simulate crack growth in loading conditions similar to those applied in the experiments.

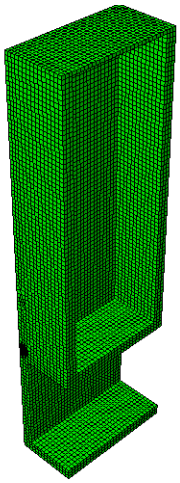

Figure 4.7: ABAQUS 3D half model of tubes

Only the portion of the HSS-1 member directly underneath the HSS-2 member was modelled because it was found that meshing the omitted region was too time consuming. The top of the HSS22 member was capped in the model geometry to facilitate load application. To further reduce the computational demand of the model, symmetry was leveraged, so only a half model was necessary.

The symmetry plane was restrained from translation in the x axis and rotation about the z axis.

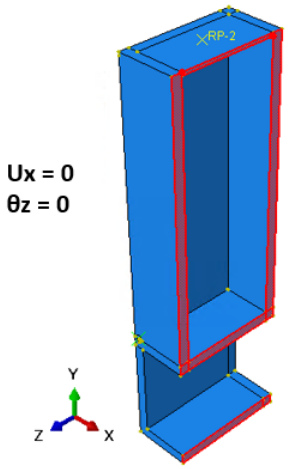

Figure 4.8: Boundary conditions for surface of symmetry of half model of tubes.

The exterior surface of the bottom flange and the HSS web were fixed in all degrees of freedom.

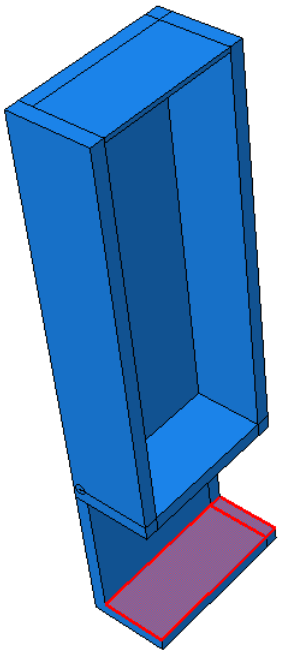

Figure 4.9: Internal surface of HSS-1 is fixed in all degrees of freedom.

The top surface of HSS-2 was constrained to a reference point at its centre to avoid localized deformation at the top surface due to load application. This is a simplification of the actual restraint condition, which was imposed by the slotted gusset plate connection. However, it results in a much simpler model and is not expected to have a significant effect on the stress state at the location of the weld.

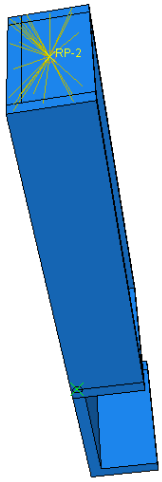

Figure 4.10: Top surface of HSS22 where plate constraint was placed.

A pressure load if 0.1778 MPa, which equates to 1 kN applied on a square surface with 75 mm dimensions, was applied to the top surface of the HSS22 member. The resulting SIF from this applied load can be related to any of the applied load ranges as the SIF will be directly proportional to the load applied due to the linear elastic nature of the material model used in the analysis.

The crack front was defined along the length of the weld propagating outwards as shown in Figure 4.11

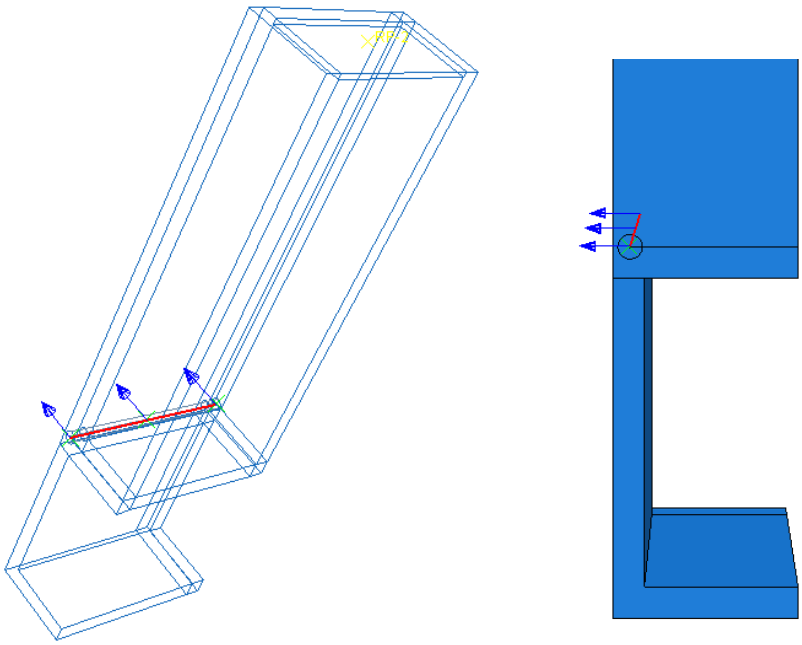

Figure 4.11: Crack front and assumed crack direction in assumed model.

A similar meshing technique was used to the 2D model that included a global mesh of half the thickness of the tubes ($t/2$) and a reduced mesh with a circular propagation in the plasticity zone surrounding the crack tip ($t/20$). The element types used were quadratic 20-node bricks with designation C3D20.

4.8 Implementing Paris' law

Table 4.1 summarized the parameters that were used in the implementation of Paris' law, in conjunction with the SIFs obtained from the 3D FE analysis.

Table 4.1: Summary of chosen parameters used in Paris' Law and their corresponding references.

Parameter	Value	Units	Ref.
σ_y	95	MPa	[29]
σ_u	240	MPa	[29]
σ_o	165	MPa	[43]
C	7.95×10^{-14}	(MPa, mm)	[45]
m	4	(MPa, mm)	[45]
ΔK_{th}	$56.7\text{-}72.3R \geq 21$	MPa$\sqrt{}$mm	[42]

4.9 Results for FEM Analysis

4.9.1 Comparison Between 2D and 3D Analysis

The results for the change in SIF along the length of the weld for a load of 45 kN, and penetration rate of 50% are plotted in Figure 4.12. The results show a parabolic distribution for the SIF with a sharp increase as location approaches the unwelded walls of HSS22 which is likely due to shear lag. Shear lag occurs in connections where not all elements of the member are attached, resulting in a non-uniform tensile stress distribution in the cross section and a concentration of stresses near the stiffer regions of the connection, which in this case translates to higher stresses at the corners of the HSS-2 member.

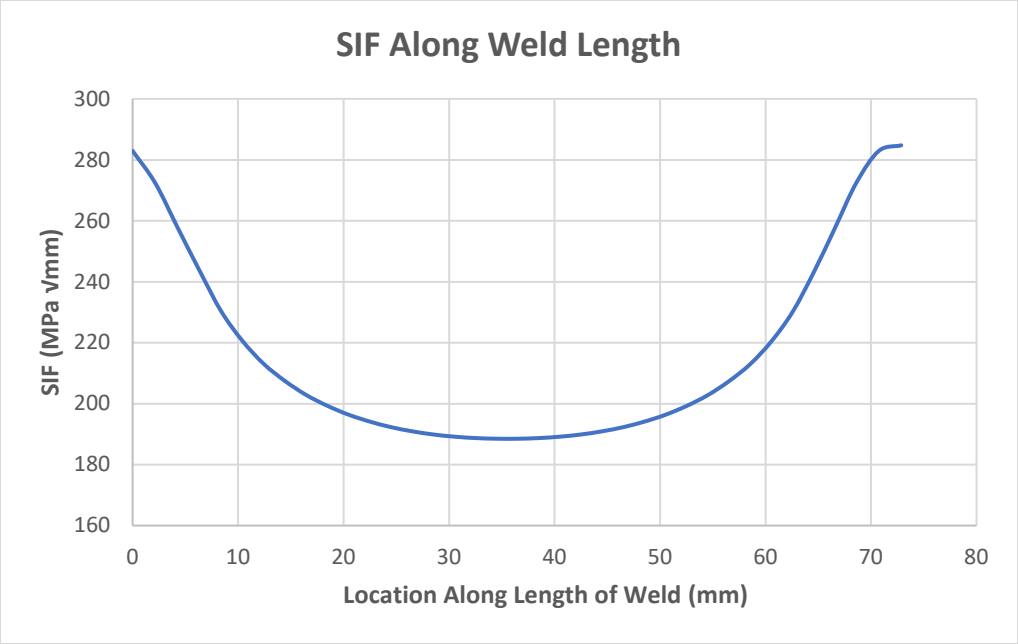

Figure 4.12: Variation of SIF along the length of the weld

The SIF distribution in Figure 4.12 is consistent with observations made in the experiments where the crack was generally seen to initiate at one of the weld ends and then propagate to the other end as shown in Figure 4.14. The SIF distribution in Figure 4.13 confirms that the primary reason for this observation is not the quality of the welds being lower at the ends, but rather the weld ends attracting higher stresses.

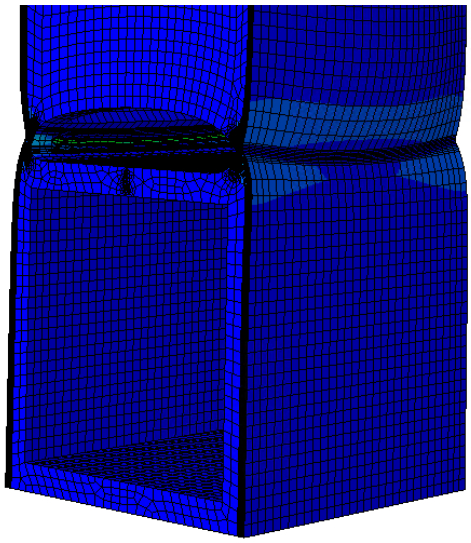

Figure 4.13: Deformed shape of tube subjected to axial loading with stress contours showing higher stresses towards the edges.

Figure 4.14: Actual weld crack propagation during an ongoing experiment starting from the edge of the specimen and propagating toward the opposite edge.

The SIF at the middle of the weld (L = 37.5 mm) should theoretically agree with the 2D plain strain behavior; however, it was found to be 188.5 MPa√mm, which differs greatly from the 2D edge crack case which results in a 420.7 MPa√mm SIF. This was likely due to the increased stiffness of the 3D geometry which prevents the walls of HSS-2 member from rotating like they did in the 2D plain strain analysis. To verify this conclusion, a second identical 2D plain stain model was constructed but with its sides restrained from translation in the horizontal axis as shown in Figure 4.15b. The resultant SIF of 168.0 MPa√mm is in closer agreement with the 3D model SIF at the middle of the wall.

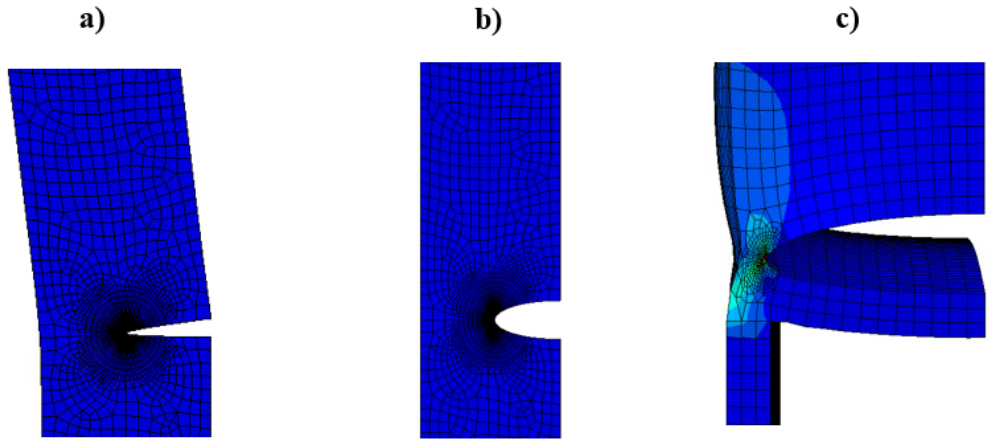

Figure 4.15: a) Deformed shape of 2D plain stain model with no horizontal restraint, b) Deformed shape of 2D plain stain model with horizontal restraint, c) Deformed shape of 3D model.

4.9.2 Comparison Between LEFM and Experimental Results

As can be seen in Figure 4.16, the LEFM analysis produces fatigue life predictions that that are more conservative than the line of best fit but lie above the design curve. The conservatism of the modelling process can be attributed to the complex propagation of the actual crack, which is simplified in the model. For example, the model assumes that both welds experience the same propagation rate while the experiments show a faster propagation at one side than the other due to slight differences in the weld quality and shape. Additionally, and perhaps more importantly, the LEFM analysis assumes that a crack starts propagating from the lack of fusion tip right from the first load cycle, with no crack initiation phase occurring first. The slope of the plotted LEFM model differs from the actual results due to the choice of Paris' law constant *m*. m is taken as 4.0 in this analysis, based on [24,41,45]. A range of values can be found for this parameter in the literature, however. Looking at the results in Figure 4.16, it would appear that a slightly better prediction could be achieved by using a slightly smaller value for *m*.

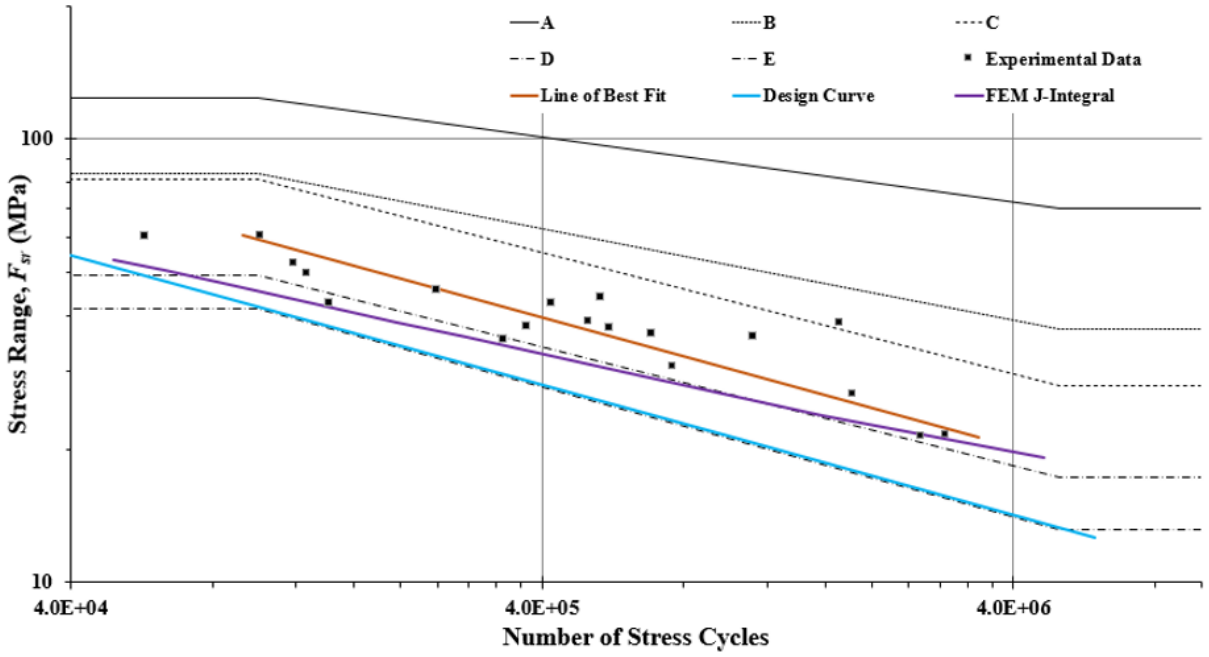

Figure 4.16: SN-Curve showing design curve obtained from the experimental data and fatigue life predictions from the LEFM approach.

5 Orthotropic Steel Decks

This chapter presents an investigation on OSD rib-deck welds undertaken to improve our understanding of how the provisions in CSA S6 and AASHTO would be implemented by a designer and to determine how the transverse wheel location affects the stresses at the weld root and toe, which can influence the location where fatigue cracks will be most likely to initiate. In the following sections of this chapter, the employed tools and methodology are first reviewed. A discussion of the results follows.

5.1 Fatigue Analysis Methods

The hotspot stress method for the fatigue assessment of welds is described and employed in Eurocode 3 [39], the well-known fatigue design recommendations by the International Institute of Weld (IIW) [38], and the Japanese JSSC standard [47]. Traditionally, the hotspot stress method has only been used to evaluate fatigue fillet welds at the toe. However, results reported in [8], [15] confirm that it can also be used for analysis of the weld root. Research efforts have also shown that the notch stress approach offers a viable solution for analyzing fillet welds of OSD rib-deck joints yielding conservative fatigue life estimates compared to the hotspot stress method. LEFM is another fatigue life prediction tool that can be used to understand fatigue behaviour during the crack propagation phase of the fatigue life of a weld. However, LEFM is highly influenced by assumed crack properties, including direction, size, and mode of propagation, which can lead to a high level of complexity in the modelling procedure.

5.1.1 Modelling Assumptions

For the current study, the refined analysis described in Clause 4.6.3.2 of AASHTO, or "Level 3 design" was employed for the analysis of local stresses at the weld at the rib-deck connection. Refined analysis is generally required for fatigue design using the hotspot stress method. In implementing the hotspot stress method, the characteristic stress of interest typically occurs at the weld root or weld toe, which are edge regions that are mesh sensitive, meaning that the stress at those points will tend to infinity, the smaller the mesh becomes. The hot spot stress method overcomes this challenge by extrapolating the stress from three points at distances $0.4 \cdot t$, $0.9 \cdot t$, and $1.4 \cdot t$ from the weld line, where t is the deck plate thickness, as shown in Figure 5.1, to obtain the characteristic stress in the region of interest.

The following expression is used to calculate the hotspot stress σ_{hs}:

$$\sigma_{hs} = 2.52 \cdot \sigma_{0.4 \cdot t} - 2.24 \cdot \sigma_{0.9 \cdot t} + 0.72 \cdot \sigma_{1.4 \cdot t} \tag{5.1}$$

where t is the deck plate thickness and the terms $\sigma_{0.4t}$, $\sigma_{0.9t}$, and $\sigma_{1.4t}$ are the stresses at the reference points

The modelling procedure implemented in this study adhered to the provisions provided in AASHTO LLRFD Clause 4.6.3.2 for a refined 3-D analysis which, include assuming:

- linear elastic material properties,
- small deflection theory,
- plane sections remain plain,
- neglecting residual stresses and imperfections, and
- idealizing weld geometry (however can be neglected for the deflection analysis).

The steel was assumed to have a modulus of elasticity of 200 GPa with no definition for yielding or plastic behaviour as fatigue stresses occurred in the linear elastic region of the material. The load applied was done as a pressure load acting on the tire contact area of 254 mm × 508 mm for both the American and Canadian trucks. The location of loads that result in the maximum deflection was obtained from an influence lines analysis and also used in the fatigue analysis.

The mesh specification as per AASHTO, requires a sufficiently meshed to resolve the pressure loading with reasonable accuracy, which was done by applying a mesh size of $t_{deck}/4$ for the deck while using a coarser mesh of $2 \cdot t_{rib}$ for the ribs. The element type used was 3-D solid continuum linear 8-noded brick elements with reduced integration with the designation C3D8R. The element size was increased further from the wheel load location, in order to minimize computation time.

Only a portion of the orthotropic deck was modelled for computational efficiency as per Clause 4.6.2.6 of the AASHTO Specification [24], which allows the use of an effective flange width for decks with $L/B < 5$ (L = 9 m, B = 12.345 m). The effective flange width was calculated to be = 2.47 m. The utilized flange width was 3.5 m to facilitate a study on the effect of varying the transverse wheel location.

The weld for the analyzed bridge deck, which was based on an actual deck system, is a partial penetration fillet weld with 80% penetration with the dimensions shown in Figure 5.1.

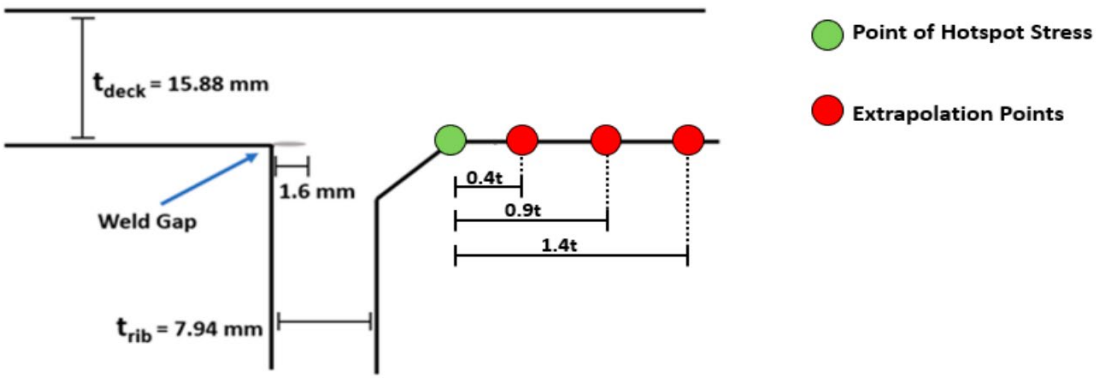

Figure 5.1: Dimensions of rib-to-deck weld with extrapolation points used in hotspot stress method.

The thickness of elements in the rib was $t/2$, while the mesh size for the deck was $t/4$. The mesh size in the region of the weld varied between $t/2$ and $t/4$. The mesh size of the weld itself is as influential as that in the extrapolation region in which the hotspot stress method is implemented.

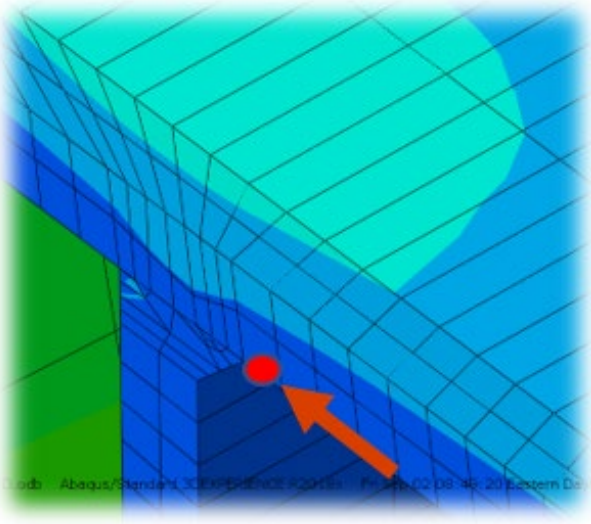

Figure 5.2: Mesh of rib-to-deck weld with red dot representing weld toe at which stress is extrapolated.

The tire contact area used is the AASHTO-prescribed 508 mm × 254 mm for both the American and Canadian cases as per CSA Clause 10.16.4. The AASHTO code prescribes a different American Truck for fatigue analysis than the one used for deflection analysis (see Figure 5.4). This is significant because the fatigue truck is about 30% longer and distributes the same weight to five axles instead of three. As noted, the CSA provisions currently require the use of the American tire contact area for fatigue analysis and instruct that we need only consider the local forces resulting from the tandem 125 kN axles the

Canadian (Figure 5.3) design axle tandem is significantly heavier (250 kN vs. 141 kN) than the American design axle (Figure 5.4) as shown in the following figures.

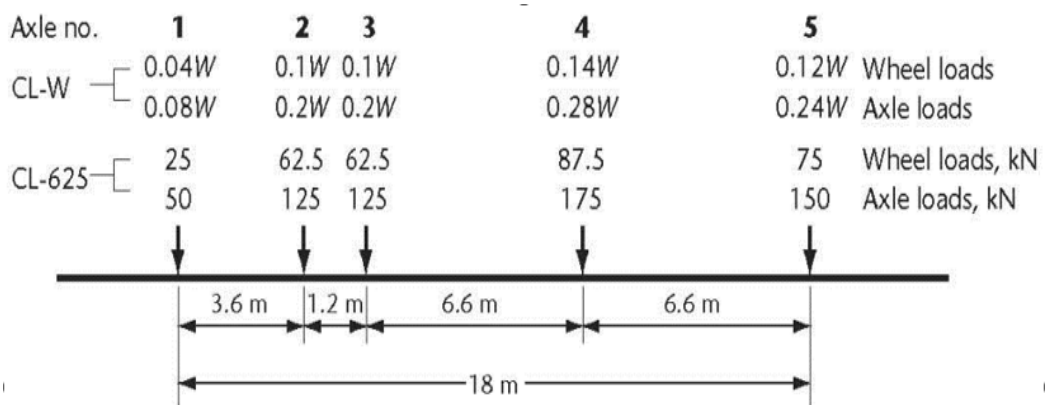

Figure 5.3: Canadian truck axle distribution[23].

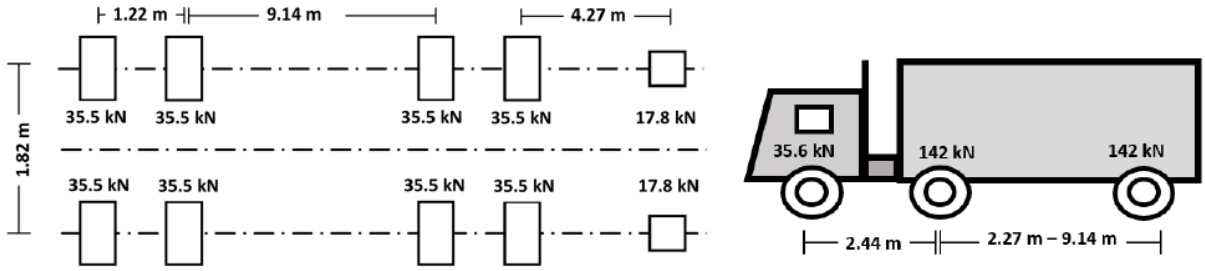

Figure 5.4:Dimensions of FLS American truck (left) and SLS and ULS American truck (right) [24].

Details of the resulting FE models, including the model boundaries and tire footprints are presented in Figure 5.5 and Figure 5.6 for the American and Canadian analysis cases, respectively.

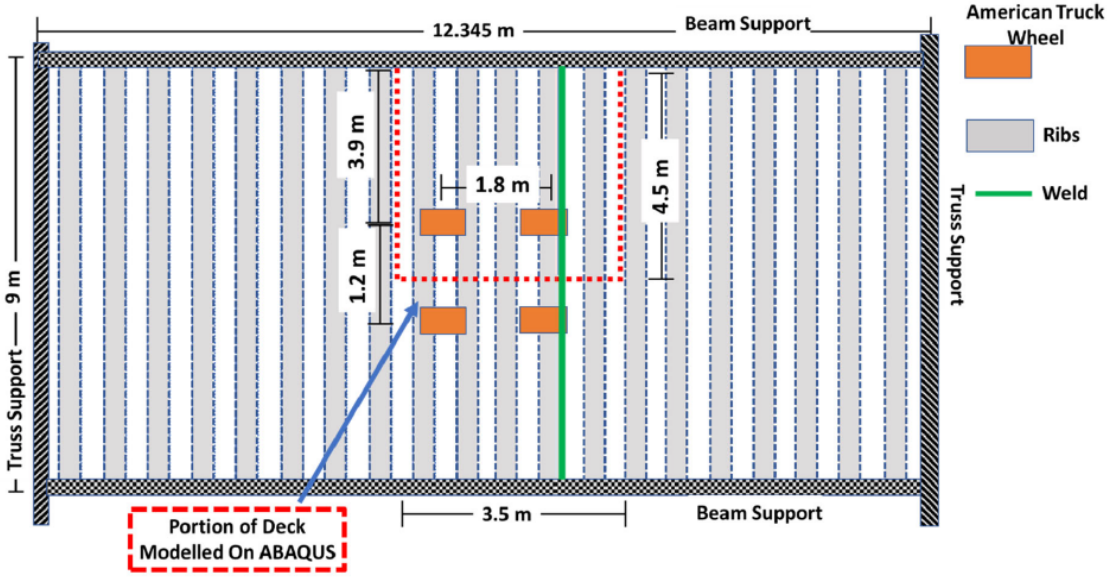

Figure 5.5:Top view of deck showing reduced geometry, weld location, and American wheel truck locations.

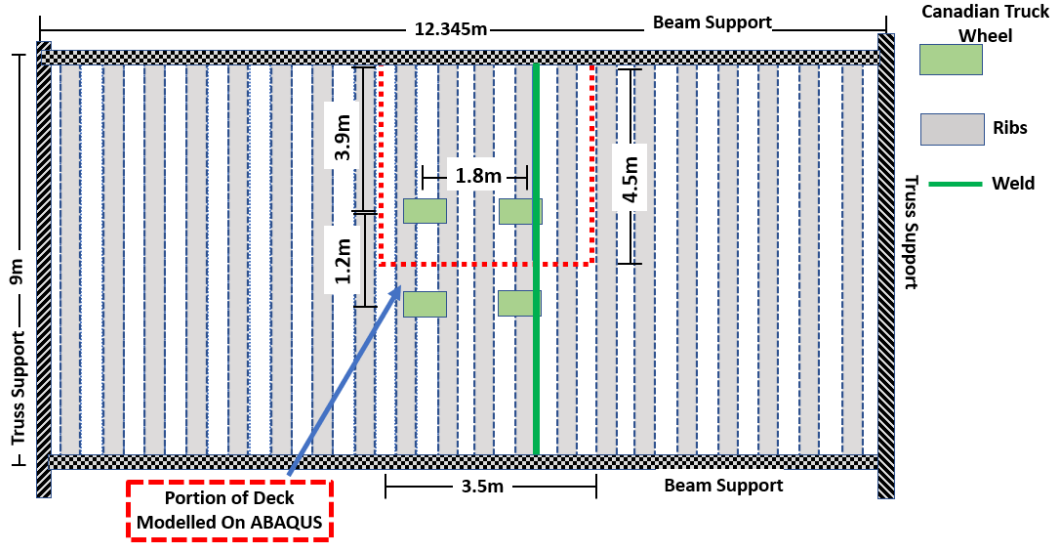

Figure 5.6: Top view of deck showing reduced geometry, weld location, and Canadian wheel truck locations.

Figure 5.7- Figure 5.9 show details the boundary conditions for the FE model used in the fatigue analysis, including those on the support line (Figure 5.7), as well as the longitudinal (Figure 5.8) and transverse (Figure 5.9) lines of symmetry. In these figures, the relevant boundaries are highlighted in red. The translational degrees of freedom are annotated as U_x, U_y, U_z, while the rotational degrees of freedom are referred to as ϑ_x ϑ_y ϑ_z.

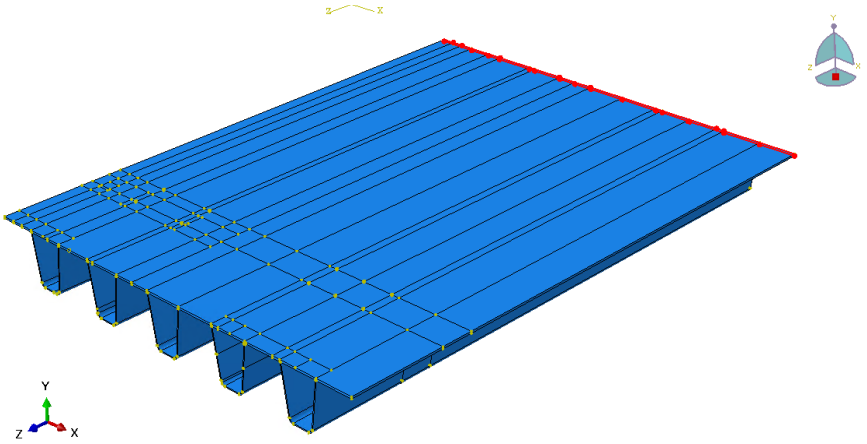

Figure 5.7: Isometric view with the pinned surface highlighted in red with the boundary conditions: $U_x = U_y = U_z = 0$.

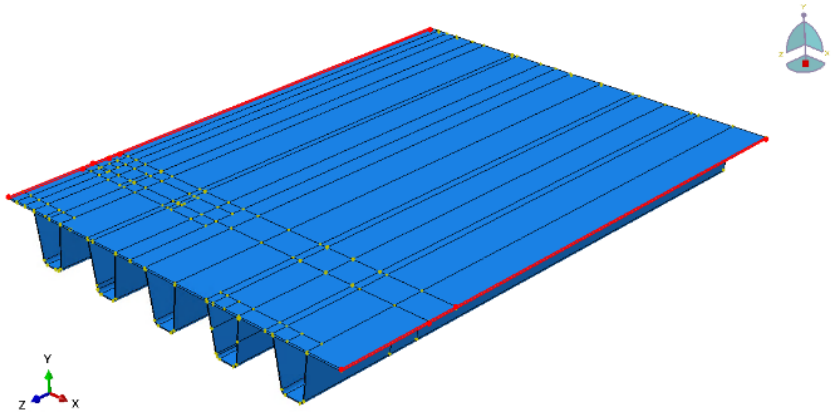

Figure 5.8: Isometric view with the sides of the deck highlighted in red with the boundary conditions: $U_x = 0$, $\vartheta_z = 0$

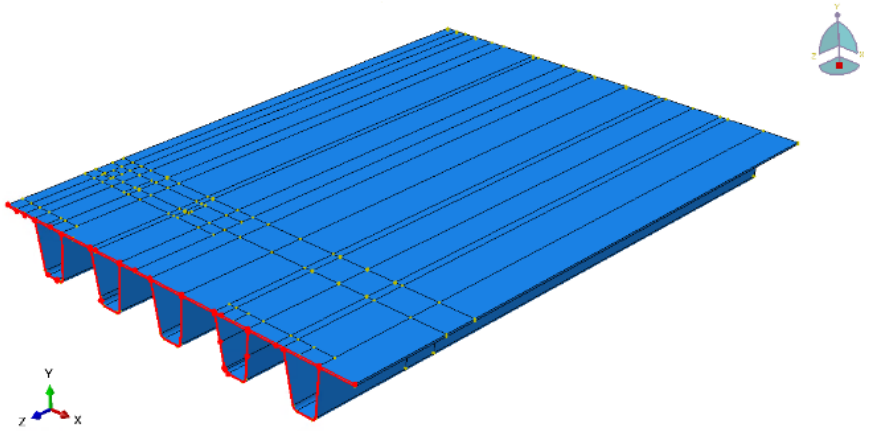

Figure 5.9: Isometric view of deck with the cut surface of the deck used to leverage symmetry: $U_z = 0$, $\vartheta_x = 0$

The deformed shapes of the fatigue loaded decks are as shown in Figure 5.10.

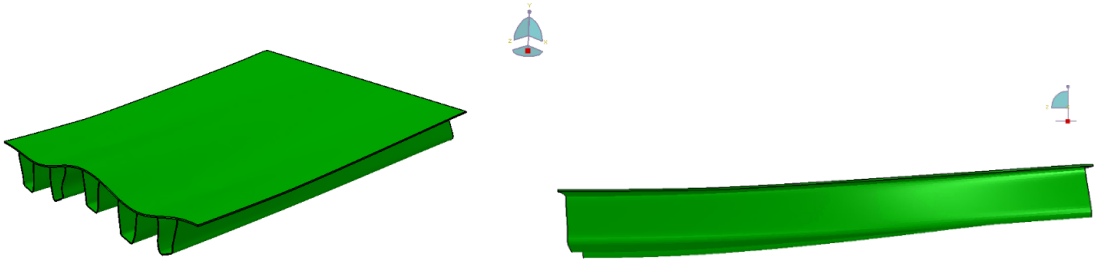

Figure 5.10: Isometric view (left) and side view (right) of deformed shape of deck.

5.2 Transverse loading

Fatigue cracking of the weld can either occur at the root or at the toe depending on the geometry of the deck and the transverse location of the load. A study was conducted by evaluating the weld stresses at the toe and root after placing the wheel load at three locations: 1) centred on top of the weld 2), centred on top of the ribs, and 3) centred in between the ribs as illustrated in Figure 5.11.

Based on the recommendations of the IIW [39] the hotspot stress method should not be used for analyzing the weld root and should only be used to analyze the weld toe. However, recent literature [8] [15] shows examples of the hotspot stress method being used for analyzing the root as well as the toe. The utilized fatigue curves to analyze the toe is FAT 100 [39] while no explicit curve is recommended for analyzing

the root. The purpose of this investigation is to find which loading scenario maximizes the stress at the toe and which loading scenario maximizes the stress at the root.

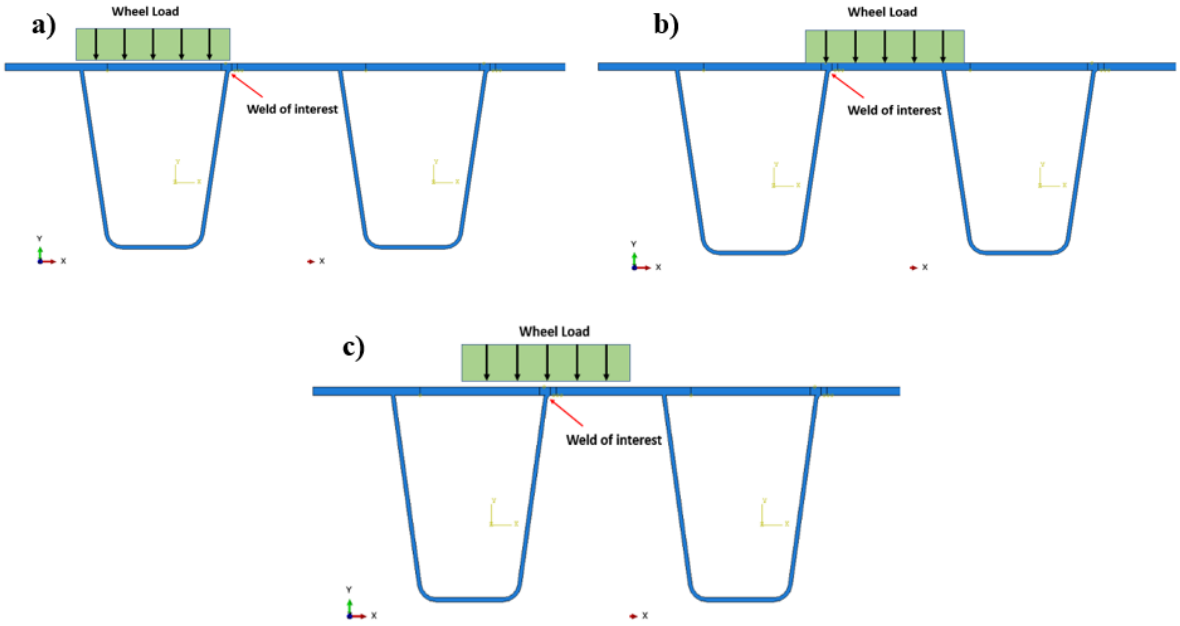

Figure 5.11: Case 1 loading scenario with load centered on top of rib, b) Case 2 loading scenario with load centered between the ribs, Case 3 loading scenario with load centered on top of weld.

5.3 Results and Discussion

This section presents the results of two studies – one conducted to compare fatigue life predictions made using the Canadian (S6) and American (AASHTO) fatigue design provisions and the other to study the effect of transverse load postion on the design stress ranges at the weld toe and root.

5.3.1 Comparative Fatigue Analysis Results

Given that the resistance curves for various fatigue detail categories in CSA S6 and AASHTO are essentially the same, the main differences between fatigue life predictions made using the two codes were expected to be in the calculated design stress ranges. The results of the comparison undertaken using the example for the Old Champlain Bridge OSD system are summarized in *Table 5.2*. In the first column of this table we see the unfactored stress ranges in MPa. Given that the Canadian design axle tandem is

significantly heavier (250 kN vs. 141 kN) and the tire load configuration is essentially the same, it is not surprising that the ratio of the unfactored stress ranges is similarly high.

Table 5.1: Summary of load factors applied by AASHTO and CSA for finite and infinite fatigue life design.

Design Type	**Finite Fatigue Life**		**Infinite Fatigue Life**	
Factor Type	**CSA**	**AASHTO**	**CSA**	**AASHTO**
Load	1.0	0.8	1.3	1.15
Dynamic	1.3	1.15	-	1.3
Reduction	0.62	-	0.5	0.571

In order to convert these unfactored stress ranges into the factored stress ranges needed for design, various load factors, dynamic load allowances, and damage equivalence factors must be applied for both finite and infinite life design (i.e., using the sloping part of the design S-N curve for low volume roads or the fatigue limit for life prediction in the very high cycle domain). These factors are summarized in *Table 5.1* and the results of their application are shown in the middle and right columns in *Table 5.2*.

Table 5.2: Results for comparative fatigue analysis between AASHTO and CSA fatigue assessment procedures using each code's respective trucks and load factors. σ-toe is the hotspot stress at the weld toe.

Fatigue Analysis at Weld Toe			
Load Case	Unfactored σ-toe (MPa)	Factored σ-toe (MPa) - Finite	Factored σ-toe (MPa) - Infinite
CAN	31.9	25.63	20.68
US	18.1	16.7	15.5
CAN/US	176%	153%	133%

From Table 5.2, it can be seen the Canadian load factors result in design stress ranges that are still higher than the American ones, the Canadian design stress range being 53% larger for finite life design and 33%

larger for infinite life design. Evaluation of the appropriatness of this difference is difficult without access to databases of current real traffic charactistics in Canada and the US, which would be needed to determine whether the Canadian traffic is more damaging from a fatigue perspective. Historical data and analysis (e.g., see [48] and Figure 5.12) suggests there are differences in the GVW spectra in Canada and the US that warrant these differences in the fatigue design stress range.

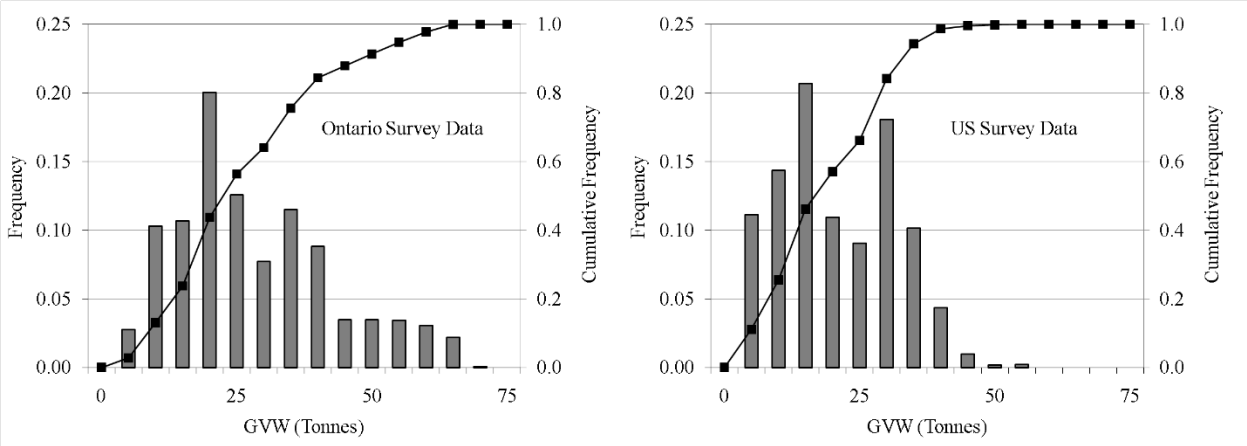

Figure 5.12: Comparison of GVW histograms from Ontario (left) and the US (right)

Perhaps the more valuable result of undertaking the comparison undertaken for this study was the appreciation that was gained regarding the lack of clarity in how the CSA S6 [23] OSD fatigue provisions should be properly implemented. The main reason for this is that AASHTO presents their damage equivalence (0.8) and infinite life threshold offset (1 / 1.75 = 0.571) factors as "load factors", which they present in Chapter 3 of their code, where loads and load factors are described. On the other hand, CSA S6 presents these factors (0.62 for finite life damage equivalence and 1 / 2 = 0.5 reduction applied to the long-life fatigue limit) as corrections embedded in the limit state functions themselves. In interpreting CSA S6, a designer who does not fully appreciate the intent of these factors could easily get confused and apply the US factors with the Canadian design tandem or apply the American adjustment factors on top of the Canadian ones, leading to overly conservative or unsafe errors, depending on what they do.

5.3.2 Transverse Loading Results

Table 5.3 presents the results of the transverse loading study, carried out to determine the importance of the wheel line location on the criticality of the weld toe and root from a fatigue perspective. From Table 5.3, it can be seen that loading Case 1 (when the load is centred over the rib) results in the maximum toe stress being 30% higher than that of Case 2 and 21% higher than the stress in Case 3. Case 3 results in the highest stress at the root being 2.5% higher than that Cases 1 and 22% higher than that Case 2.

Table 5.3: Results for varying transverse locations of a Canadian design truck load.

Stress at Wheel Load (MPa)			
	Case 1	Case 2	Case 3
σ-Toe	35.1	27.0	29.0
σ-Root	31.4	26.3	32.2

No informative conclusions can be drawn about comparisons between the root and toe stress as no fatigue curve has been recommended for the hotspot stress at the root of the weld. In order to do such a comparison, a notch stress approach is recommended in AASHTO, but no notch stress design curve is given. To find such a design curve, the IIW Recommendation [39] can be referenced. However, notch stress analysis of the weld root was not attempted within the scope of the current study.

6 Conclusions and Future Work

6.1.1 Summary

Partial joint penetration (PJP) and partial penetration flare bevel groove (FBG) welds can be a cost-effective option compared to full penetration welds and can be advantageous in certain situations. They are particularly useful in cases where the stress on the weld is relatively low or significant cyclic loading is not anticipated, such as for welds in pedestrian bridges with hollow structural sections. However, it can be challenging to assess the fatigue performance of these welds, due to limitations and lack of knowledge concerning existing methods for fatigue design in these applications. PJP welds can also be beneficial in scenarios where a full penetration weld is difficult or impractical, such as for thin-walled components like the rib-to-deck welds of OSDs. Current provisions in CSA S6-19 Clause 10.16 require the design of OSDs to satisfy the requirements of Clause 9.8.3 of AASHTO LRFD Bridge Design Specifications while still using loads and factors from CSA S6-19 for the fatigue limit state (FLS). Due to the difference in applied factors and loads, there are instances when attempting to use this approach incorrectly can lead to possible negative outcomes from the point of view of structural safety or economy.

Against this background, a study was conducted to address current gaps in the literature regarding the fatigue performance of PJP and partial penetration FBG welds for bridge applications.

The experimental fatigue testing of 19 T-joint aluminum FBG welded specimens, conducted within the scope of this study, yielded valuable insights into the fatigue behavior of these components. Notably, the effective throat was found to be the most important factor influencing the performance of FBG welds, and it was found that precision in the welding execution is crucial. An SN curve was established based on the experimental results for a 95% survival probability. The weld performance based on the design curve was found to be similar to Detail Category E in CSA S6-19. Linear elastic fracture mechanics (LEFM) methods were then used, along with a 3D finite element (FE) model, to supplement the experimental study and predict the fatigue performance of the tested aluminum FBG welds. Lastly, an investigation was conducted on OSD rib-deck welds to determine how the transverse wheel location affects the stress at the root and toe. In order to address the ambiguity issues identified in CSA S6-19, the local stresses resulting from Canadian and American trucks were computed and compared.

6.1.2 Conclusions Concerning Aluminum FBG Welds

This first study was conducted to address a current gap in the literature regarding the fatigue performance of partial penetration FBG welds. The experimental fatigue testing of 19 aluminum specimens has yielded

valuable insights into the fatigue behavior of these components. Certain parameters were varied in this experimental study to investigate their effects on performance. These parameters included the corner radius of the hollow section and the specimen size (overall dimensions).

An analysis of the test results indicates the most influential parameter on the joint performance is the effective throat, as this performance is largely dependent on the stress of the weld. This highlights the importance of welding precision and geometry control for FBG welds. Consequently, increasing the corner radius can improve the joint performance as the resulting weld throat is larger.

By plotting the experimental results on an SN curve, drawing the line of best fit, and then offsetting it based on a 95% survival probability, a design curve was obtained for this weld to aid engineers in determining the expected fatigue life under axial loading conditions. The resulting design curve showed that performance of the weld is approximately the same as Detail Category E in CSA S6-19.

A linear elastic fracture mechanics (LEFM) model was then used, along with a 3D finite element (FE) model employing the J-integral method, to predict the fatigue performance of this joint type. This model was used to simulate the stress distribution and crack propagation in the specimens under axial loading conditions, and the results were compared to the SN curve generated from the experimental data. It is worth noting that the results from the FE model were in good agreement with the test data, resulting in a curve that lies between the experimental line of best fit and obtained design curve.

6.1.3 Conclusions Concerning PJP welds in OSDs

In the second study, a comparison between the weld toe stresses in an OSD rib-to-deck weld resulting from different design trucks showed that the Canadian truck results in stresses that are 53% and 33% higher for finite and infinite life fatigue design, respectively. The transverse location of the wheel loads is an influential parameter on the fatigue stresses in the weld. Based on the obtained results, two loading scenarios should be investigated by placing the wheel load centered on top of the ribs to maximize the toe stress and centered on top of the weld to maximize the root stresses.

To provide clarity on when to use the Canadian or American factors while calculating the fatigue design stress range, it is suggested that CSA S6 guidelines be followed. However, for information on the modelling aspects (such as effective flange width calculation) and resistance categories of various fatigue details, AASHTO should be referenced. This approach is simple because the AASHTO fatigue detail categories (A, B, C, etc.) use similar S-N curves to the CSA categories. Additionally, the dynamic load allowance, damage equivalence factor, and reduction factors for fatigue design are based on Canadian research and calibration efforts, making them more appropriate for Canadian traffic.

To assess the weld root fatigue in the PJP rib-to-deck plate weld, AASHTO proposes employing the notch stress approach. However, no resistance curve is specified. The IIW design curve and the CSA S6 Detail Category A design curve were compared as two viable options, and it was found that the two curves are reasonably close with latter being slightly more conservative.

6.2 Future Work

Based on the presented research, the following areas for future work are identified:

- Future research on FBG welds in aluminum tubular joint applications could investigate more complex geometries such as K-joints also common in pedestrian bridges.
- Fillet welds between tube ends and base plates are a similar detail common to highway accessory (e.g., light pole, sign) structures, where weld root cracking is also critical and cyclic loading from wind and traffic-induced gusts is possible – application of the methods used in this thesis could be of interest for establishing suitable design approaches for these details.
- Another area where research is still needed is assessing what is an appropriate fatigue loading model for pedestrian bridges where FBG welds and tubular joints are used.
- Additional research could help enhance our understanding of how the level of penetration (LOP) affects the fatigue performance of the rib-to-deck weld in an OSD. As achieving an accurate LOP and assessing it accurately through non-destructive examination methods is challenging, a performance-based approach that informs the designer of when an achieved LOP is fatigue-acceptable or not could potentially reduce fabrication costs.
- Further research is recommended to investigate the use of the notch stress approach to provide fatigue life predictions for the root in the rib-to-deck weld of an OSD. This could include experimental verification of this approach and an investigation on how to use this approach to accurately model the effects on fatigue performance of varying the LOP level.
- Further research is required to quantify the actual frequency and weight of trucks that would pass over an OSD in Canada. One challenge observed here is that the studies typically being done related to gross vehicle weight (GVW) and ultimate limit state (ULS) design may not be directly applicable to fatigue damage prediction for OSDs, where heavy axle groups and lighter but more frequent trucks may have a much more significant influence on fatigue damage.

References

[1] R.J. Connor, J.W. Fisher, W. Gatti, V. Gopalaratnam, B. Kozy, B. Leshko, D.L. McQuaid, R. Medlock, D. Mertz, T. Murphy, D. Paterson, O. Sorensen, J. Yadlosky, Manual for design, construction, and maintenance of orthotropic steel 484 deck bridges, Report No. FHWA-IF-12-027, US Department of Transportation Federal Highway Administration, Washington, D.C., USA, 2012.

[2] D. Wang, C. Xiang, Y. Ma, A. Chen, and B. Wang, "Experimental study on the root-deck fatigue crack on orthotropic steel decks," *Mater Des*, vol. 203, May 2021, doi: 10.1016/j.matdes.2021.109601.

[3] B. Ji, R. Liu, C. Chen, H. Maeno, and X. Chen, "Evaluation on root-deck fatigue of orthotropic steel bridge deck," *J Constr Steel Res*, vol. 90, pp. 174–183, 2013, doi: 10.1016/j.jcsr.2013.07.036.

[4] Z. G. Xiao, K. Yamada, S. Ya, and X. L. Zhao, "Stress analyses and fatigue evaluation of rib-to-deck joints in steel orthotropic decks," *Int J Fatigue*, vol. 30, no. 8, pp. 1387–1397, Aug. 2008, doi: 10.1016/j.ijfatigue.2007.10.008.

[5] Q. Zhang, "Review on Fatigue Problems of Orthotropic Steel Bridge Deck Design and Evaluation of Bridges with Improved Mechanical Performance and Sustianability View project," 2017. [Online]. Available: https://www.researchgate.net/publication/317779510

[6] S. Ya, K. Yamada, and T. Ishikawa, "Fatigue Evaluation of Rib-to-Deck Welded Joints of Orthotropic Steel Bridge Deck," *Journal of Bridge Engineering*, vol. 16, no. 4, pp. 492–499, Jul. 2011, doi: 10.1061/(asce)be.1943-5592.0000181.

[7] K. Yamada, S. Ya, Plate bending fatigue tests for root crack of trough rib of orthotropic steel deck, J. Struct. Eng. 54 (2008) 675–684.

[8] Z. Fu, B. Ji, C. Zhang, and D. Li, "Experimental study on the fatigue performance of roof and U-rib welds of orthotropic steel bridge decks," *KSCE Journal of Civil Engineering*, vol. 22, no. 1, pp. 270–278, Jan. 2018, doi: 10.1007/s12205-017-1725-0.

[9] M. Li, Y. Suzuki, K. Hashimoto, and K. Sugiura, "Experimental Study on Fatigue Resistance of Rib-to-Deck Joint in Orthotropic Steel Bridge Deck," *Journal of Bridge Engineering*, vol. 23, no. 2, Feb. 2018, doi: 10.1061/(asce)be.1943-5592.0001175.

[10] W. Nagy, Fatigue Assessment of Orthotropic Steel Decks Based on Fracture Mechanics, Ghent University, Belgium, 2017

[11] S. Kainuma, M. Yang, Y. S. Jeong, S. Inokuchi, A. Kawabata, and D. Uchida, “Experiment on fatigue behavior of rib-to-deck weld root in orthotropic steel decks,” *J Constr Steel Res*, vol. 119, pp. 113–122, Mar. 2016, doi: 10.1016/j.jcsr.2015.11.014

[12] H.-B. Sim and C.-M. Uang, “Stress analyses and parametric study on full-scale fatigue tests of rib-to-deck welded joints in steel orthotropic decks,” *Journal of Bridge Engineering*, vol. 17, no. 5, pp. 765–773, 2012.

[13] S. Kainuma, M. Yang, Y. S. Jeong, S. Inokuchi, A. Kawabata, and D. Uchida, “Experimental investigation for structural parameter effects on fatigue behavior of rib-to-deck welded joints in orthotropic steel decks,” *Eng Fail Anal*, vol. 79, pp. 520–537, Sep. 2017, doi: 10.1016/j.engfailanal.2017.04.028.

[14] M.H. Kolstein Fatigue classification of welded joints in orthotropic steel bridge decks Delft University of Technology, TU Delft (2007).

[15] H. Yang, P. Wang, H. Qian, and P. Dong, “Fatigue performance of different rib-to-deck connections using traction structural stress method,” *Applied Sciences (Switzerland)*, vol. 10, no. 4, Feb. 2020, doi: 10.3390/app10041239.

[16] J. W. Fisher and J. M. Barsom, “Evaluation of Cracking in the Rib-to-Deck Welds of the Bronx–Whitestone Bridge,” *Journal of Bridge Engineering*, vol. 21, no. 3, Mar. 2016, doi: 10.1061/(asce)be.1943-5592.0000823.

[17] S. Kainuma, M. Yang, Y.-S. Jeong, S. Inokuchi, A. Kawabata, and D. Uchida, “Fatigue Behavior Investigation and Stress Analysis for Rib-to-Deck Welded Joints in Orthotropic Steel Decks,” International Journal of Steel Structures, vol. 18, no. 2, pp. 512–527, Apr. 2018, doi: 10.1007/s13296-018-0067-1

[18] H.-B. Sim, C.-M. Uang, and C. Sikorsky, “Effects of Fabrication Procedures on Fatigue Resistance of Welded Joints in Steel Orthotropic Decks”, doi: 10.1061/ASCE1084-0702200914:5366.

[19] B. Cao, Y. Ding, F. Geng, and A. Li, “Parametric Study and Fatigue Life Evaluation Using Effective Notch Stress Approach for Rib-to-Deck Welded Joints in Orthotropic Steel Decks,” *Journal of Performance of Constructed Facilities*, vol. 35, no. 3, Jun. 2021, doi: 10.1061/(asce)cf.1943-5509.0001584.

[20] C. Xiang, D. Wang, B. Wang, A. Chen, and R. Ma, “Numerical simulation of root-deck crack propagation of orthotropic steel bridge deck,” *Structure and Infrastructure Engineering*, vol. 18, no. 7, pp. 1076–1090, 2022, doi: 10.1080/15732479.2022.2039219.

[21] W. Wu, H. Kolstein, and M. Veljkovic, “Fatigue resistance of rib-to-deck welded joint in OSDs, analyzed by fracture mechanics,” *J Constr Steel Res*, vol. 162, Nov. 2019, doi: 10.1016/j.jcsr.2019.105700

[22] X. Ju and K. Tateishi, “Fatigue Crack Behavior at Rib-To-Deck Weld Bead in Orthotropic Steel Deck,” Advances in Structural Engineering, vol. 17, no. 10, pp. 1459–1468, Nov. 2014, doi: 10.1260/1369-4332.17.10.1459.

[23] Canadian Highway Bridge Design Code, CSA S6, 2019

[24] AASHTO LRFD Bridge Design Specifications. Washington, D.C.: American Association of State Highway and Transportation Officials, 2017.

[25] G. Zhao, C. C. Fu, Y. Lu, and T. Saad, “Fatigue assessment of highway bridges under traffic loading using microscopic traffic simulation,” *Bridge Optimization - Inspection and Condition Monitoring*, 2020.

[26] Deloitte, “Life Cycle Analysis Aluminium vs. Steel,” tech. rep., 2012.

[27] G. Laurent, “Partial Joint Penetration Welds in Aluminum Structures” Master’s thesis, Department of civil and environmental engineering, University of Waterloo, Waterloo, Ontario 2020.

[28] J.-P. *European recommendations for the design of simple joints in steel structures, [Eurocode 3, part 1-8*. [Brussels]: ECCS European Convention for Constructional Steelwork, 2009. ISBN 92-9147-000-95.

[29] CSA, Strength design in aluminum / Commentary on CSA S157-17 , Strength design in aluminum. 2018.

[30] The Aluminum Association, Aluminum Design Manual. 2015.

[31] European Committee for Standardization, Eurocode 9: Design of aluminium structures - Part 1-1: General structural rules. 2007.

[32] R. Schiller, M. Oswald, J. Neuhäusler, K. Rother, and I. Engelhardt, “Fatigue strength of partial penetration butt welds of mild steel,” *Welding in the World*, vol. 66, no. 12, pp. 2563–2584, 2022.

[33] S. Kim, K. Jin, W. Sung, and S. Nam, “Effect of Lack of Penetration on the fatigue strength of high strength steel butt weld,” KSME Journal, vol. 8, no. 2, pp. 191–197, 1994.

[34] F. V. Lawrence and W. H. Munse, “Fatigue Crack Propagation in Butt Welds Containing Joint Penetration Defects,” Welding Journal (Miami, Fla), vol. 52, no. 5, pp. 221–225, 1973.

[35] N. Hiroshi, M. Eto, K. Tachibana, and M. Nakahira, “Fatigue strength reduction factor of partial penetration weldments for ITER vacuum vessel,” in SMiRT 16: Selected and Updated

Papers from the 16th International Conference on Structural Mechanics in Reactor Technology, Washington, DC, no. August, 2001.

[36] J. Burk and F. V. Lawrence, “Effects of Lack-of-Penetration and Lack-of-Fusion on the Fatigue Properties of 5083 Aluminum Alloy Welds,” tech. rep., University of Illinois at Urbana-Champaign, 1976.

[37] U. Brandt, F. V. Lawrence, and C. M. Sonsino, “Fatigue crack initiation and growth in AlMg4.5Mn butt weldments,” Fatigue and Fracture of Engineering Materials and Structures, vol. 24, no. 2, pp. 117–126, 2001.

[38] C. M. Sonsino, D. Radaj, U. Brandt, and H. P. Lehrke, “Fatigue assessment of welded joints in AlMg 4.5Mn aluminum alloy (AA 5083) by local approaches,” International Journal of Fatigue, vol. 21, no. 9, pp. 985–999, 1999.

[39] A. Hobbacher Recommendations for Fatigue Design of Welded Joints and Components International Institute of Welding (2002) (IIW doc. XIII-1539-96/XV-845-96)

[40] European Committee for Standardization. EN 1993-2:2006. Eurocode 3: Design of steel structures. Part 2: Steel bridges. Brussels (Belgium); 2006

[41] Standard, A. I. S. C. Specification for Structural Steel Buildings, 2016.

[42] A. F. Hobbacher, Recommendations for Fatigue Design of Welded Joints and Components. International Institute of Welding, 2014.

[43] J. C. Newman, “A crack opening stress equation for fatigue crack growth,” International Journal of Fracture, vol. 24, no. 4, pp. 131–135, 1984.

[44] R. C. McClung, “Finite Element Analysis of Specimen Geometry Effects on Fatigue Crack Closure,” Fatigue & Fracture of Engineering Materials & Structures, vol. 17, no. 8, pp. 861–872, 1994.

[45] R. Ranjan, K. Ghahremani, S. Walbridge, and A. Ince, “Testing and fracture mechanics analysis of strength effects on the fatigue behavior of HFMI-treated welds,” Welding in the World, vol. 60, no. 5, pp. 987–999, 2016.

[46] T. L. Anderson, Fracture Mechanics: Fundamentals and Applications, Fourth Edition. 2017.

[47] JSSC (Japanese Society of Steel Construction), 2012. Fatigue design recommendations for steel structures, Gihodo Shuppan, Tokyo.

[48] R. Coughlin, S. Walbridge, (2011). Fatigue correction factors for welded aluminum highway structures. Canadian journal of civil engineering, 38(10), 1082-1091.